TRIUMF Experiment E614
Technical Note #65

GARFIELD Simulation of the TEC

V.I.Selivanov
03 May 2002

Abstract

TEC with DME and ISO gas was simulated and optimized using GARFIELD 7.08 program. An influence of all outside conditions on TEC parameters has been estimated. Three different locations of the TEC are possible: close to a fringe field area, in area of the second focus F2 of the M13 beam line, and inside of the E614 magnet at B=2T. Further GEANT calculations are needed for the TEC location optimization.

1 TEC at B=0

1.1 TEC geometry

Drawing of an optimized TEC is shown in Fig.1. The TEC consists of two parts. Muons cross the drift area of the TEC restricted to the cathode, strips, and grid wire planes. Strip voltages has been selected to provide an homogeneous electric field inside the drift area. Electrons from a tracking particle move along X-axis (electric field direction) to an amplification area beginning behind the grid wire plane and collect on sense wires. Distance between sense (and grid) wires was 1mm. Proposed design of 2D ETC is shown in Fig.2. Input window of the TEC Gas-Box must have thickness $> 6\mu m$ of mylar because a proton at $p = 29.8MeV/c$ has range of $6\mu m$ in mylar according to PSTAR program [http://physics.nist.gov/PhysRefData/Star/Text/PSTAR.html]. Rate ratio of $p/\mu^+ \geq 20$ has been measured at $p = 29.8MeV/c$ for the M13 beam line [C.J.Oram, J.B.Warren, G.Marshall, J.Doornbos, D.Ottewell "M13 Beam Line Tuning", Preprint TRIUMF TRI-80-1 (1980)].

1.2 Edge effects

Program GARFIELD 7.08 has been used for calculations. The calculations has been done for DME(C_2H_6O) and ISO(iC_4H_{10}) gases at pressure of $40Torr$. Details of the calculations are described in Section 5. TEC box consists wires only because the program allows using not more than two infinite planes. Wires with diameter of $150\mu m$ have imitated the continuous planes represented in Fig.1. More than 900 wires been used for the TEC description. Wires with length of 100cm been selected. The used TEC geometry is shown in Fig.3 together with $V = const$ contours. Influence of outside charged objects on electrical field inside the TEC has been estimated. Fig.4 presents contours $V = const$ for a system consists of the TEC and an additional strips plane placed on distance of $5mm$ outside the TEC strips plane. This outside strips plane has voltage distribution opposite to the nearest TEC strips plane direction. Maximal used value of $V_c = -4300V$ has been selected. No influence of the plane on the electric field distribution inside the TEC volume has been obtained.

Edge effects has been investigated and optimized. Drift lines of electrons from a track are shown in Fig.5 at $V_c = -2000V$ with DME gas. First sense wire placed at Y=-1.6cm. One can see some drift line distortion near the lower edge of the TEC volume. Arrival drift time distributions of electrons from the track are shown in Fig.6 at $V_c = -2000V$ and in Fig.7 at $V_c = -4300V$. One can see a delay of drift time about 3ns near the edge at $V_c = -2000V$ and much less delay about 0.2ns at $V_c = -4300V$. This edge effect was calculated with distance of $0.5mm$ also between the grid wires.

The delay is practically zero for this case at any values of V_c. Gain changing near the TEC edge is shown in Figs.8-9. The changing is less than 20% for the both values of V_c. Values of $V_g = 950V$ and $V_g = 1130V$ were selected for DME and ISO gas correspondingly to have gain $\approx 10^4$.

1.3 Drift parameters

Drift parameters of the TEC has been calculated using a track with length of 1-1.3mm in Y-axis direction covering the central wire space. Electron drift lines for the track are shown in Figs.10-11. Arrival time distributions along the track are shown in Figs.12-13. One can see that the drift time spread is $\simeq 5ns$ for DME gas and $\simeq 3.5ns$ for ISO gas. The numbers are much smaller than a diffusion spread of electrons in both gases (see below). Gain distributions along the track are shown in Figs.14-15. The gain spread is about 4% for ISO gas and 10% for DME gas. A gain was calculated also for a track going along $Y = 0$ axis. One can see from Fig.16 that the gain begins practically from the grid wire plane placed at $X = 0.3cm$ on horizontal axis of the Fig.16.

Dependence of the TEC resolution from value of V_c was calculated using "single cluster" case when a single drift electron placed with a equal probability along a track. The track has length of $1mm$ and direction along Y-axis. It covers the central wire cell only. A diffusion of the electron in a gas gives for this case a maximal contribution to the TEC resolution. An example of an arrival time distribution of electrons from the track together with the fitting curve is shown in Fig.17. Figs.18-19 present dependence of a space resolution from value of V_c for DME and ISO gas respectively. One can see from Figs.18-19 that the TEC resolution has a week dependence from an electric field in the drift space. Figs.20-21 and 22-23 demonstrate a drift velocity and maximum drift time dependence for the both gases. Value of $V_c = 2000V$ was selected for further calculations with ISO gas. Space resolution of the TEC with DME gas was calculated at $V_c = 2000V$ and $V_c = 4300V$.

Space resolution of the TEC at selected values of the V_c was calculated using the HEED subprogram of GARFIELD. The program calculates all interactions of a particle with gas and drift of electrons from the primary particle and secondary γ-quantum and δ-electrons. Typical tracks of μ^+ and e^+ at $p = 29.8MeV/c$ are presented in Figs.24-25. Cluster distribution from a surface muon for DME and ISO gas is presented in Figs.26-27. The surface muon produces $3.6e^- \cdot mm^{-1}$ and $7.6e^- \cdot mm^{-1}$ in DME and ISO gas respectively. Fig.28 presents surface muon energy loss distribution per cluster.

Relation between the position of a track and the drift time ($t(x)$-relation) was calculated using "ARRIVAL-TIME-DISTRIBUTION" command (see Section 5). The position d has counted out the grid wire plane. Several tracks with different position (travel distance) have been simulated using the HEED subprogram. The tracks have direction along Y-axis and length of $1mm$ covering the central wire space. 20000 tracks were simulated at each travel distance. Arrival time distribution of a second electron from a track was simulated and fitted as that was presented in Fig.17. Figs.29-30 present $t(x)$-relations for DME and ISO gases. Mean value of a fitting curve at each travel distance d together with its error of σ was used for the fitting. Figs.31-32 present dependence of the TEC spatial resolution from the travel distance d.

1.4 Influence of outside conditions on TEC parameters

Influence of values V_c, V_s, pressure p, temperature T, magnetic field B, and an ion space charge on drift velocity, gain, and t_0 has been calculated as that was described above. t_0 is a parameter describing $t(x)$-relation in Figs.29-30. Drift gas data have been calculated at several values of pressure p, temperature T, and magnetic field B. Values of V_{drift}, gain, and t_0 depend linearly on p, V_c, V_s and T, for example:

$$\Delta V_{drift}/V_{drift} = \alpha \cdot \Delta V_c; \qquad \Delta t_o = \alpha \cdot \Delta V_c. \tag{1}$$

Drift velocity V_{drift} only depends from B quadratically:

$$\Delta V_{drift}/V_{drift} = -\alpha^2 \cdot \Delta B. \tag{2}$$

Tables 1-9 present the influence of outside conditions on TEC parameters with DME and ISO gas at $p = 40 Torr$.

Table 1: Drift velocity shift. DME gas, B=0, $V_g - V_c = 4300V$.

Source of the shift	$\Delta(V_s - V_g)$	$\Delta(V_g - V_c)$	Δp	ΔT	ΔB	Space charge
α	$< 10^{-5}$ $/10V$	$2.9 \cdot 10^{-5}$ $/V$	$-4.1 \cdot 10^{-3}$ $/Torr$	$2.4 \cdot 10^{-4}$ $/^{\circ}C$	$4.8 \cdot 10^{-3}$ $/kG$	–
$(*) \pm 100 \mu m$	–	$> \pm 30V$	$\pm 0.5 Torr$	$> \pm 8^{\circ}C$	$0.65 kG$	$\mu^+ rate$ $\simeq 5 \cdot 10^4 s^{-1}$
$(**) \pm 5 mr$	–	$> \pm 30V$	$\pm 2 Torr$	$> \pm 8^{\circ}C$	$> 1 kG$	–

$(*)$ Max. shift of reconstructed distance on $\pm 100 \mu m$ corresponds to
$(**)$ Max. shift of reconstructed angle ($50 mr$) on $\pm 5 mr$ corresponds to

Table 2: Gain shift. DME gas, B=0, $V_g - V_c = 4300V$.

Source of the shift	$\Delta(V_s - V_g)$	$\Delta(V_g - V_c)$	Δp	ΔT	ΔB
α	$2.9 \cdot 10^{-2}/V$	0	$-0.29/Torr$	0	0
$(*) \pm 20\%$	$\pm 7V$	–	$\pm 0.7 Torr$	–	–

$(*)$ Gain shift on $\pm 20\%$ corresponds to

Table 3: t_0 shift. DME gas, B=0, $V_g - V_c = 4300V$.

Source of the shift	$\Delta(V_s - V_g)$	$\Delta(V_g - V_c)$	Δp	ΔT	ΔB
$\alpha(ns)$	$< 10^{-3}/V$	$< 2 \cdot 10^{-3}/V$	$-0.69/Torr$	$1.4 \cdot 10^{-2}/^{\circ}C$	$< 0.3/kG$
$(*) \pm 100 \mu m$	–	–	$\pm 3 Torr$	–	–

$(*)$ Max. shift of reconstructed distance on $\pm 100 \mu m$ corresponds to

Table 4: Drift velocity shift. DME gas, B=0, $V_g - V_c = 2000V$.

Source of the shift	$\Delta(V_s - V_g)$	$\Delta(V_g - V_c)$	Δp	ΔT	ΔB	Space charge
α	$< 10^{-5}$ $/10V$	$1.4 \cdot 10^{-4}$ $/V$	$-1.8 \cdot 10^{-3}$ $/Torr$	$4.8 \cdot 10^{-4}$ $/^\circ C$	$1.1 \cdot 10^{-2}$ $/kG$	–
$(*) \pm 100\mu m$	–	$> \pm 10V$	$\pm 1Torr$	$> \pm 8^\circ C$	$0.45kG$	$\mu^+ rate$ $\simeq 10^4 s^{-1}$
$(**) \pm 5mr$	–	$> \pm 10V$	$\pm 3Torr$	$> \pm 8^\circ C$	$> 2kG$	–

(∗) Max. shift of reconstructed distance on $\pm 100\mu m$ corresponds to
(∗∗) Max. shift of reconstructed angle ($50mr$) on $\pm 5mr$ corresponds to

Table 5: Gain shift. DME gas, B=0, $V_g - V_c = 2000V$.

Source of the shift	$\Delta(V_s - V_g)$	$\Delta(V_g - V_c)$	Δp	ΔT	ΔB
α	$2.9 \cdot 10^{-2}/V$	0	$-0.29/Torr$	0	0
$(*) \pm 20\%$	$\pm 7V$	–	$\pm 0.7Torr$	–	–

(∗) Gain shift on ±20% corresponds to

Table 6: Drift velocity shift. ISO gas, B=0, $V_g - V_c = 2000V$.

Source of the shift	$\Delta(V_s - V_g)$	$\Delta(V_g - V_c)$	Δp	ΔT	ΔB	Space charge
α	$< 10^{-5}$ $/10V$	$3.1 \cdot 10^{-5}$ $/V$	$-2.3 \cdot 10^{-3}$ $/Torr$	$4.5 \cdot 10^{-4}$ $/^\circ C$	$1.3 \cdot 10^{-2}$ $/kG$	–
$(*) \pm 100\mu m$	–	$> \pm 20V$	$\pm 1.2Torr$	$> \pm 8^\circ C$	$0.25kG$	$\mu^+ rate$ $\simeq 5 \cdot 10^3 s^{-1}$
$(**) \pm 5mr$	–	$> \pm 20V$	$\pm 5Torr$	$> \pm 10^\circ C$	$> 0.5kG$	–

(∗) Max. shift of reconstructed distance on $\pm 100\mu m$ corresponds to
(∗∗) Max. shift of reconstructed angle ($50mr$) on $\pm 5mr$ corresponds to

Table 7: Gain shift. ISO gas, B=0, $V_g - V_c = 2000V$.

Source of the shift	$\Delta(V_s - V_g)$	$\Delta(V_g - V_c)$	Δp	ΔT	ΔB
α	$3.2 \cdot 10^{-2}/V$	0	$-0.23/Torr$	0	0
$(*) \pm 20\%$	$\pm 6V$	–	$\pm 0.9Torr$	–	–

(∗) Gain shift on ±20% corresponds to

Influence of an ion space charge in drift area of the TEC on value of V_{drift} was calculated using article D.Friedrch, G.Melchart, B.Sadoulet, F.Sauli "Positive ion effects in large-volume drift chambers", Nucl. Instr. Meth., 158 (1979) 81-88. Ion drift lines from a sense wire are shown in Fig.33 for

DME gas at $V_c = -2000V$ for TEC at B=0, and in Fig.34 for DME gas for TEC at B=2T. About 15% of ions penetrate from the amplification to the drift area. The penetration ratio of 50% was used for estimations. Total drift time of ions at B=0 is about $20ms$ at $V_c = -2000V$ and $10ms$ at $V_c = -4300V$. Total drift time of ions in TEC at B=2T is about $5ms$. Calculated requirement on a maximum muon rate is shown in Tables 1, 4, 6, 8.

2 TEC at B=2T

TEC can be placed in B=2T area as a first element of E614 detector itself. An one dimension TEC sees a muon helix projection. A muon helix at B=2T has period about $30cm$ and amplitude $R(mm) = 5 \cdot 10^{-2} \cdot \theta(mr)$, where θ is a polar angle of a muon helix because a muon depolarization before and after fringe field area. For example, the crucial for us value of $\theta = 15mr(1 - P_\mu = 10^{-4})$ corresponds to $R = 0.75mm$. One dimension TEC with length of $20cm$ covering more than half of a muon helix period is proposed for measurements. Drawing of the TEC is shown in Fig.35. The TEC construction at B=2T is identical to the TEC at B=0, but width of the drift area is $23mm$ and the total TEC length is $200mm$. Electron drift lines in Z=0 plane from a track are shown in Fig.36. The TEC has a drift area space of $2.3cm$ covering a muon beam space with a spread of $\theta = \pm 100mr$. Dependence of single electron space resolution of the TEC versus value of V_c for several travel distances d is shown in Fig.37. Figs.38-39 demonstrate dependence of drift velocity and a maximal drift time of the TEC from the d at $V_c = -2000V$. t(x)-relation and dependence of space resolution from a travel distance d are shown in Figs.40-41. Drifting electron moves outside of XY-plane because a Lorentz drift angle. Muon track and a trajectory of drifting electrons in $Z = 0$ and $Y = 0$ planes calculated by HEED subprogram are shown in Figs.42-43. Muon track on the Figs. moves from X=0.8cm along Y-axis. An intrinsic scattering of the muon track is about $2.5mr$.

Influence of outside conditions on TEC parameters at B=2T with DME gas is shown in Tables 8-9.

Table 8: Drift velocity shift. DME gas, B=2T, $V_g - V_c = 2000V$.

Source of the shift	$\Delta(V_s - V_g)$	$\Delta(V_g - V_c)$	Δp	ΔT	ΔB	Space charge
α	$< 10^{-5}$ $/10V$	$4.2 \cdot 10^{-5}$ $/V$	$-2.3 \cdot 10^{-2}$ $/Torr$	$4.5 \cdot 10^{-4}$ $/°C$	$6.4 \cdot 10^{-5}$ $/0.1kG$	–
$(*) \pm 100\mu m$	–	$> \pm 10V$	$\pm 0.12Torr$	$> \pm 8°C$	$> 0.4kG$	$\mu^+ rate$ $\simeq 7 \cdot 10^4 s^{-1}$
$(**) \pm 5mr$	–	$> \pm 20V$	$\pm 0.5Torr$	$> \pm 10°C$	$> 0.5kG$	–

$(*)$ Max. shift of reconstructed distance on $\pm 100\mu m$ corresponds to
$(**)$ Max. shift of reconstructed angle ($50mr$) on $\pm 5mr$ corresponds to

Table 9: Gain shift. DME gas, B=2T, $V_g - V_c = 2000V$.

Source of the shift	$\Delta(V_s - V_g)$	$\Delta(V_g - V_c)$	Δp	ΔT	ΔB
α	$2 \cdot 10^{-2}/V$	0	$-0.27/Torr$	0	0
$(*) \pm 20\%$	$\pm 10V$	–	$\pm 0.7Torr$	–	–

$(*)$ Gain shift on $\pm 20\%$ corresponds to

3 Discussion

Tables 10, 11 present drift parameters for all calculated TECs.

Table 10: TEC parameters.

	DME gas, B=0, $V_g - V_c = 4300V$	DME gas, B=0, $V_g - V_c = 2000V$	ISO gas, B=0, $V_g - V_c = 2000V$	DME gas, B=2T, $V_g - V_c = 2000V$
Beam square, (mm)	48×48	48×48	48×48	23×23
Number of sense wires	48	48	48	200
$V_s - V_g, (V)$	950	950	1130	950
Gain, (10^4)	1.1	1.1	1.3	1.1
Number of electrons, $(mm^{-1})(*)$	3.6	3.6	7.9	3.6
$P(\geq 1e^-), (\%)(**)$	95.2	95.2	99.8	95.2
$P(\geq 2e^-), (\%)(***)$	80.7	80.7	93.3	80.7
Drift velocity, $(\mu m/ns)$	58.40	46.78	54.99	15.54 $(\star)$
$t_{max}, (\mu s)$	0.82	0.95	0.89	1.6
Average resolution, $(\mu m)(\star\star)$	340	340	220	120
Accuracy of position reconstruction, (μm)	49	49	32	8.5
Accuracy of angle reconstruction, (mr)	2.9	2.9	1.9	0.12

$(*)$ Calculated by HEED program for μ^+ at $p = 29.8MeV/c$
$(**)$ Probability to register $\geq 1e^-$
$(***)$ Probability to register $\geq 2e^-$
$(\star)$ Component in plane orthogonal to wire direction
$(\star\star)$ Resolution in center of TEC for a surface muon at threshold of $1.5e^-$

Table 11: Requirement to the TEC operation parameters.

Requirement	$\Delta(V_s - V_g)$, (V)	$\Delta(V_g - V_c)$, (V)	Δp, $(Torr)$	ΔT, $(^\circ C)$	ΔB, (kG)	$\mu^+ rate$, (s^{-1})
DME, B=0, $V_g - V_c = 4300V$	$< \pm 7$	$< \pm 30$	$< \pm 0.5$	$< \pm 8$	< 0.65	$< 5 \cdot 10^4$
DME, B=0, $V_g - V_c = 2000V$	$< \pm 7$	$< \pm 10$	$< \pm 0.7$	$< \pm 8$	< 0.45	$< 10^4$
ISO, B=0, $V_g - V_c = 2000V$	$< \pm 6$	$< \pm 20$	$< \pm 0.9$	$< \pm 8$	< 0.25	$< 5 \cdot 10^3$
DME, B=2T, $V_g - V_c = 2000V$	$< \pm 10$	$< \pm 10$	$< \pm 0.12$	$< \pm 8$	< 0.4	$< 7 \cdot 10^4$

The 2D TEC at B=0 must be placed closer as possible to the fringe field area to decrease an influence of an intrinsic gas scattering on muon depolarization by the fringe field. The shortest distance is defined by an influence of B_z-component of fringe field (B_r-component is small) on value of V_{drift} in drift area of the TEC. DME gas at $V_c = -4300V$ is best case because the B_z-component can reach value of $0.65kG$ compare with $0.25kG$ for ISO gas at $V_c = -2000V$.

Average space resolution of TEC with ISO gas is about $220\mu m$ compare with $340\mu m$ for DME gas, but a real resolution will be defined by a multiple scattering of muon in 6 mylar foils of 2D TEC construction and in gas. GEANT simulation could estimate a real decreasing of P_μ-value.
Both gases provide a sufficient registration efficiency at a really accessible threshold of $1.5e^-$.
Ion space charge in a TEC with square of $48 \times 48mm^2$ restricts allowed muon rate. A high value of V_c is preferable.
A second location of the 2D TEC is possible at the second focus F2 inside M13 beam line. Muon scattering by the 2D TEC provides a minimal contribution of the scattering to P_μ-value.
Muon track reconstruction using the 2D TEC at B=0 requests a knowledge of the track position respect to magnetic field map and a fringe field distribution with a sufficient accuracy. One can only calculate a final value of P_μ after fringe field area using reconstructed track position respect to magnetic field and the fringe field distribution. It is a disadvantage of course.
1D TEC with length of $20cm$ at B=2T allows a helix track reconstruction with needed accuracy. Requirement to gas pressure stability of $\pm 0.12Torr$ is a disadvantage of this case. The TEC measures a muon polar angle θ and radius R of a helix after fringe field area. The measured values define completely value of P_μ without a knowledge of the fringe field distribution and position of a muon track respect to magnetic field. It is a direct measurement of P_μ value for each muon.

4 TEC calibration

Drift parameters of TEC obtained from the GARFIELD have a some precision. An experimental calibration may be essential to check the calculation results. Slits with width of $0.5mm$ through $10mm$ placed before and after of each 2D TEC could provide a calibration of the 2D TEC at B=0. Tungsten with thickness of $0.16mm$ could be used for this device manufacturing.

TEC calibration at B=2T can be done using particles with $\theta \approx 0$ after the fringe field area. This calibration is needed at two TEC positions as minimum. Protons with $p = 120MeV/c$ could be useful for the calibration to decrease an influence of a helix radius on reconstruction results. A typical proton track at $p = 120MeV/c$ is shown in Fig.44.

5 Details of GARFIELD calculations

Calculation of gas data has been done using MAGBOLTZ 2 subprogram with MONTE-CARLO-INTEGRATION providing most accurate calculations of all drift parameters. One can see below examples of this part of the program. Calculated drift parameters are shown in Figs.45-56. A diffusion coefficient along drift direction marked by $(*)$ and orthogonal to drift direction marked by $(\circ)$ in Figs.51, 52, 54. Fig.53 presents components of $\overrightarrow{V}_{drift}$ vector in a local coordinate system when the magnetic field, B, is taken along the X-axis and the electric field, E, is at an angle, Φ in the X-Z plane. Components V_x, V_y, V_z marked by $(*), (+), (\circ)$ respectively. Ion mobility in DME and ISO gas equals to $0.56 \cdot 10^{-6}$ and $0.614 \cdot 10^{-6}$ respectively.

****Gas data calculated by below file have been used for TEC simulation at B=0.

.

.

```
&GAS
GLOBAL mob=0.56e-6
opt gas-pl
pressure 40 Torr
temperature 294 K
MAGBOLTZ DME 100.0 E/P-RAN 0.01 5000.0 log-E/P-scale N-E/P 200 ...
B-FIELD 0.0 ...
monte-carlo-integration collisions 80 mobility {mob}
HEED DME 100
write {DME_B0_P40_T294.DAT80}
.
.
```

****Gas data calculated by below file have been used for TEC simulation at B=2T.

```
.
.
&MAGNETIC
components 0.0 2.0 0.0 tesla
&GAS
pressure 60 Torr
temperature 294
GLOBAL mob=0.56e-6
opt gas-pl
pressure 40 Torr
temperature 294 K
MAGBOLTZ DME 100.0 E/P-RAN 0.1 5000.0 log-E/P-scale N-E/P 200 ...
B-FIELD 2.0 ...
angle-range 0.0 90.0 n-angle 10 ...
monte-carlo-integration collisions 20 mobility {mob}
HEED DME 100
opt gas-pl
write {DME_B2_00_P40_T294.DAT20}
.
.
```

Ordinary GARFIELD 7.08 has been used for calculations. Careful tuning of "INTEGRATION-PARAMETERS" section only is needed for the correct calculations.

****The below file has been used for an accuracy TEC calculations.

```
.
.
&DRIFT
INTEGRATION-PARAMETERS ...
integration-accuracy 1.0E-9 ...
diffusion-accuracy 1.0E-7 ...
townsend-accuracy 1.0E-5 ...
diffusion-stack-depth 5 ...
townsend-stack-depth 5 ...
interpolation-order 2 ...
maximum-step-length 0.02 ...
```

CLOUD-PROJECTION-DISTANCE 5000.0 ...
calculate-if-interpolation-fails
*abandon-if-interpolation-fails
.

List of Figures

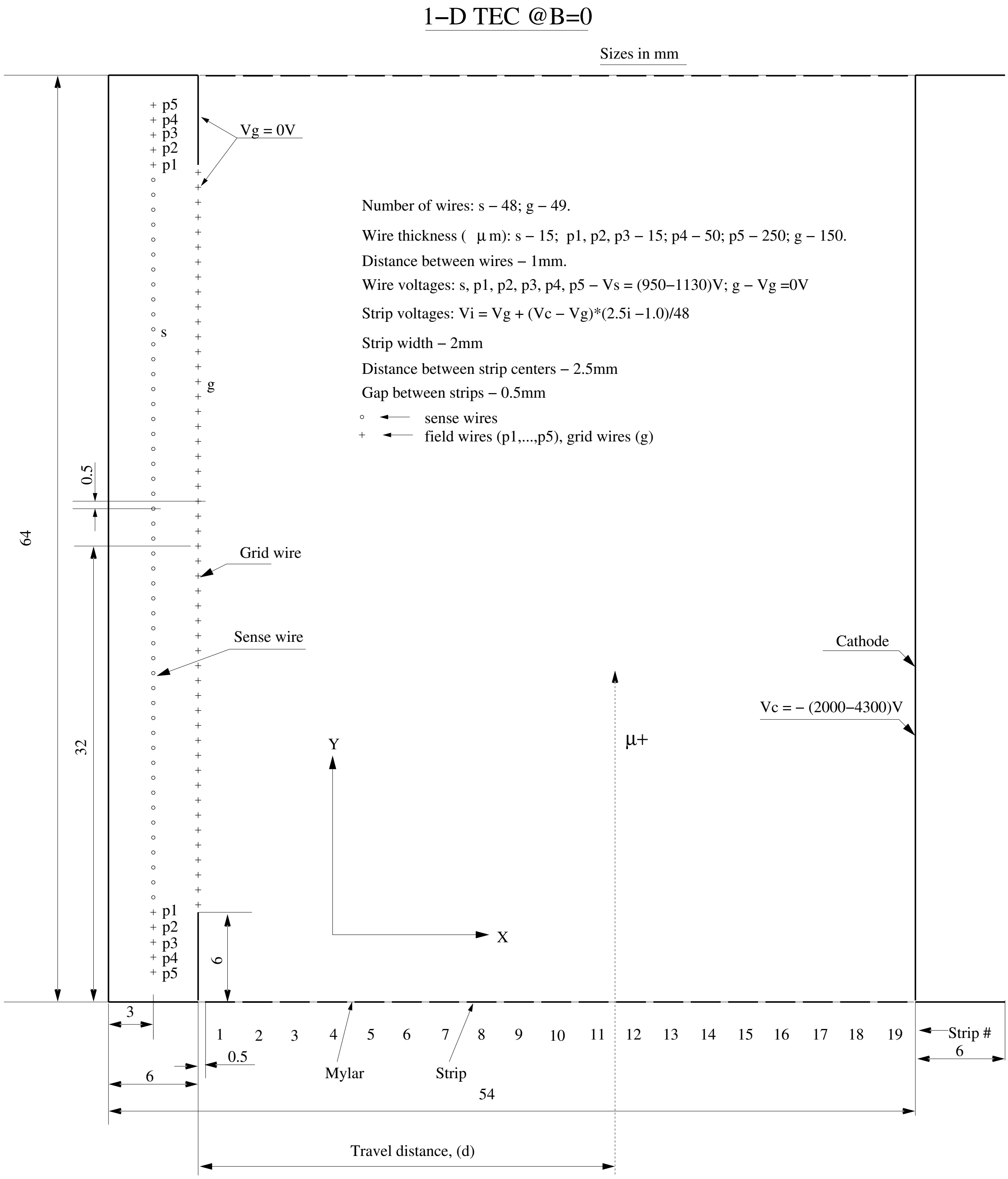

Figure 1: TEC view in XY-plane. Length of the TEC in Z direction is 100 cm.

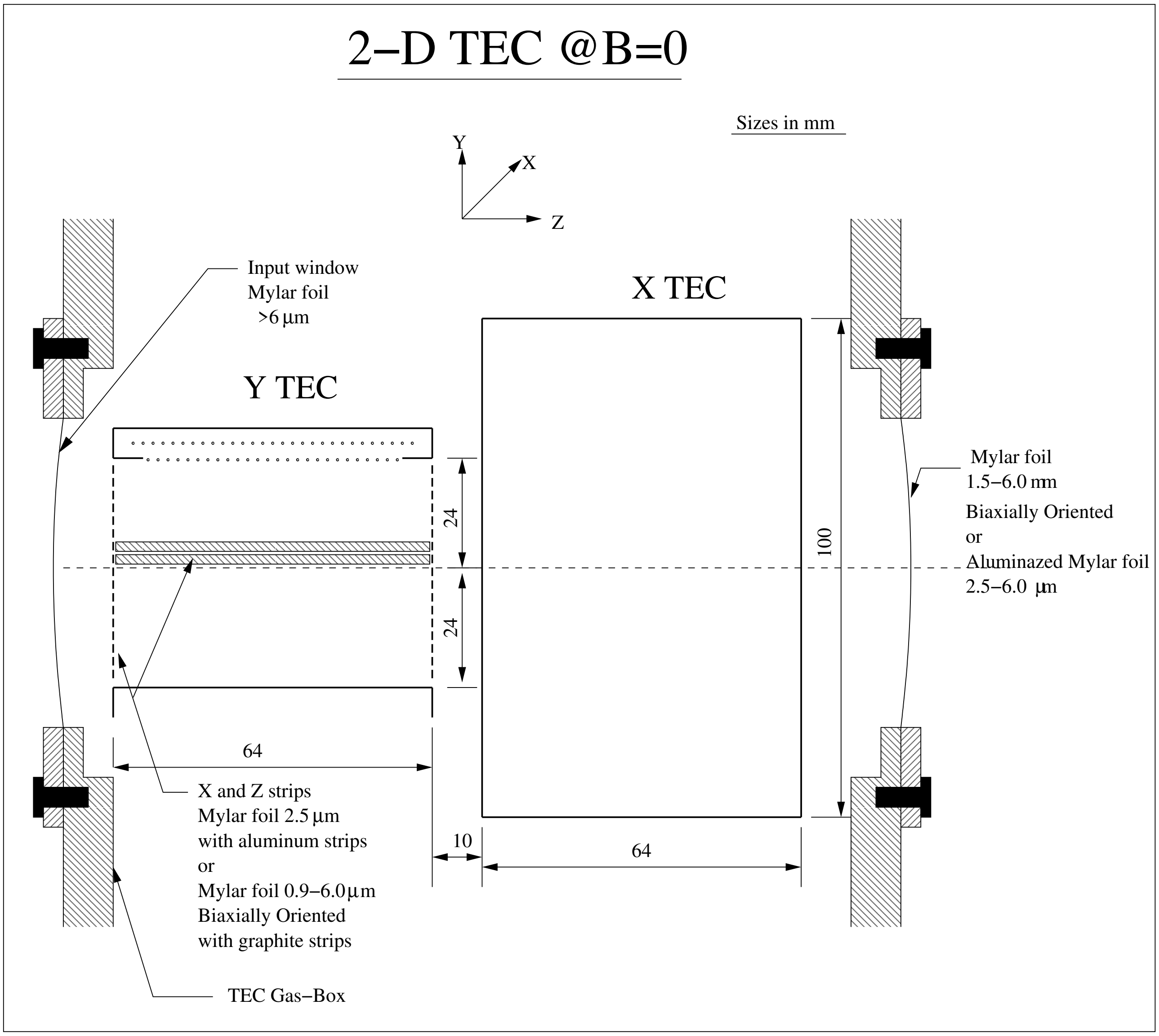

Figure 2: Sketch of 2D TEC system at B=0.

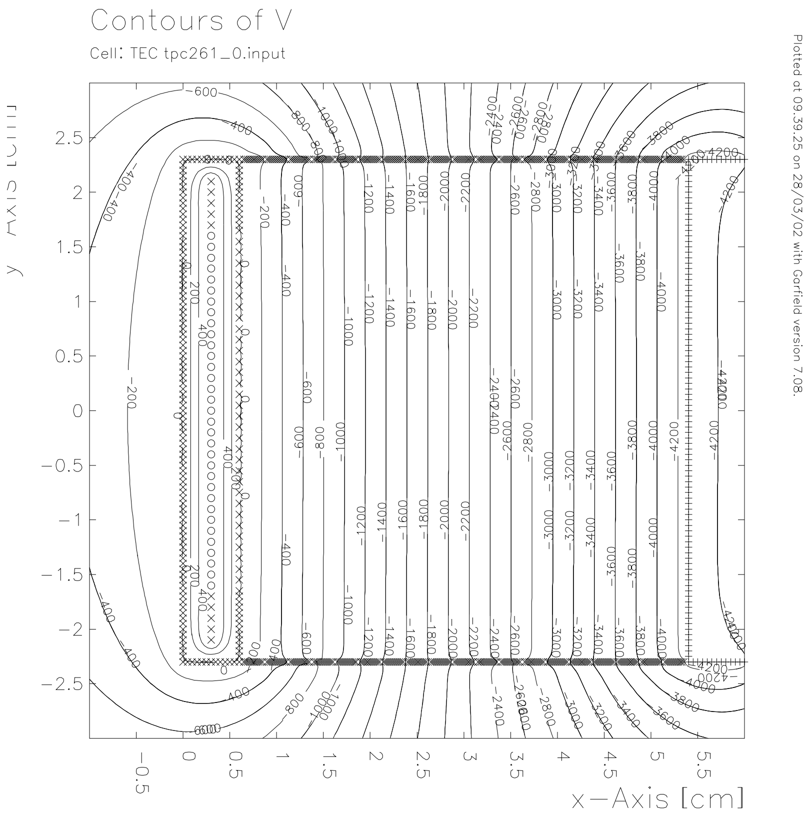

Figure 3: The TEC view in XY-plane together with contours of V=const.

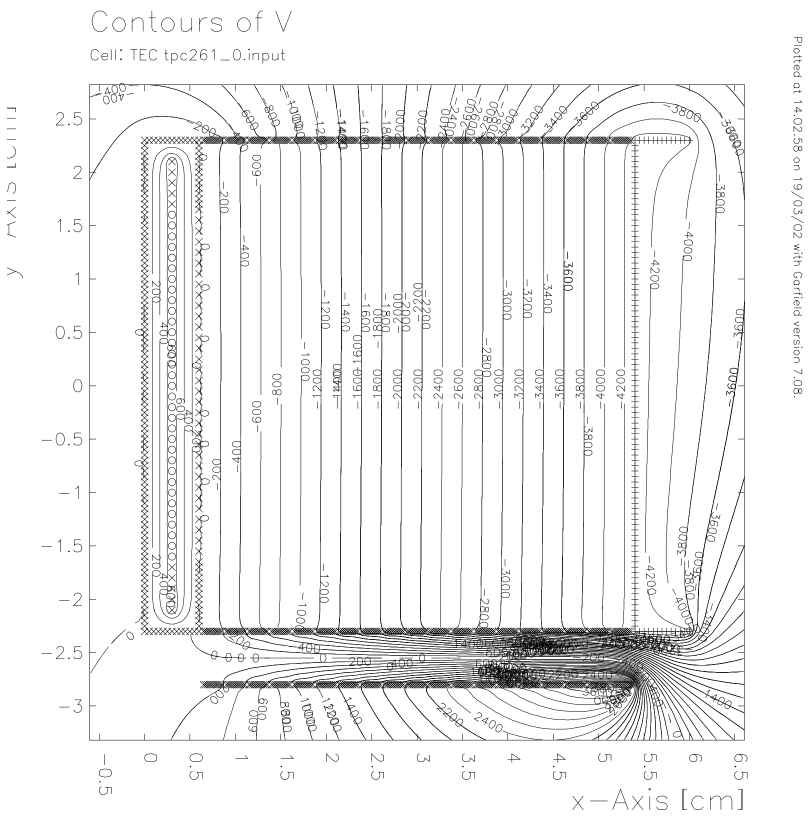

Figure 4: Contours of V=const for the TEC with the additional outside strips plane.

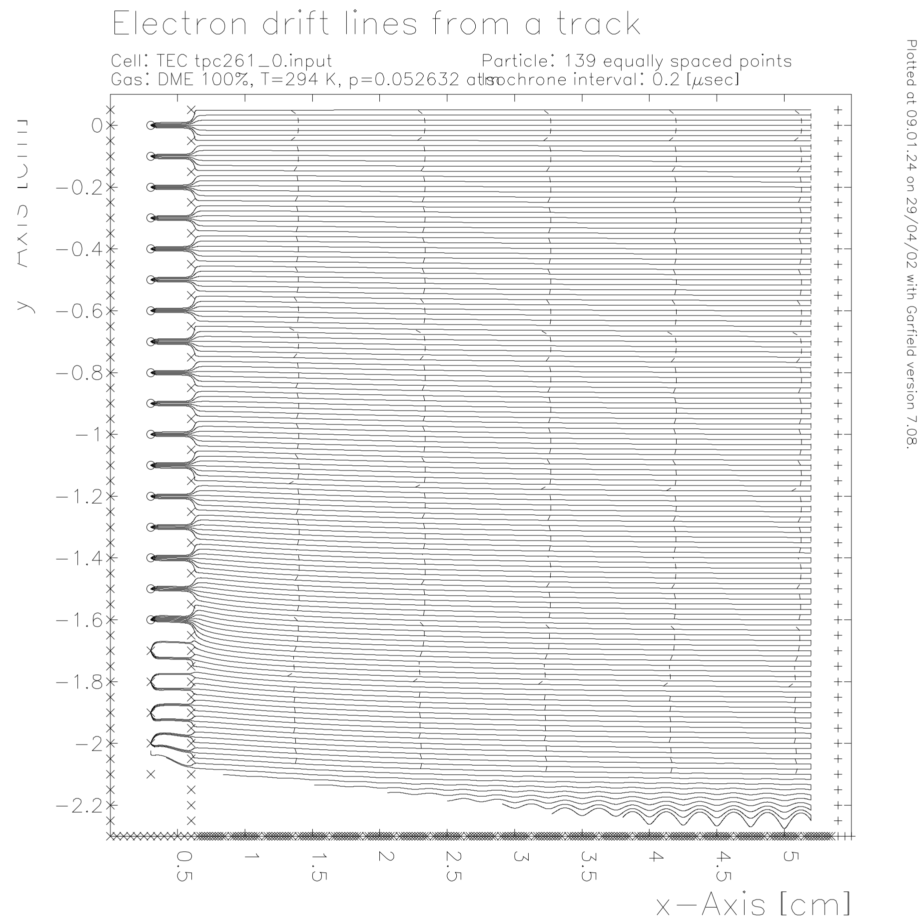

Figure 5: Drift lines from a track. DME gas, $V_c = -2000V$, no diffusion. First sense wire placed at Y=-1.6cm.

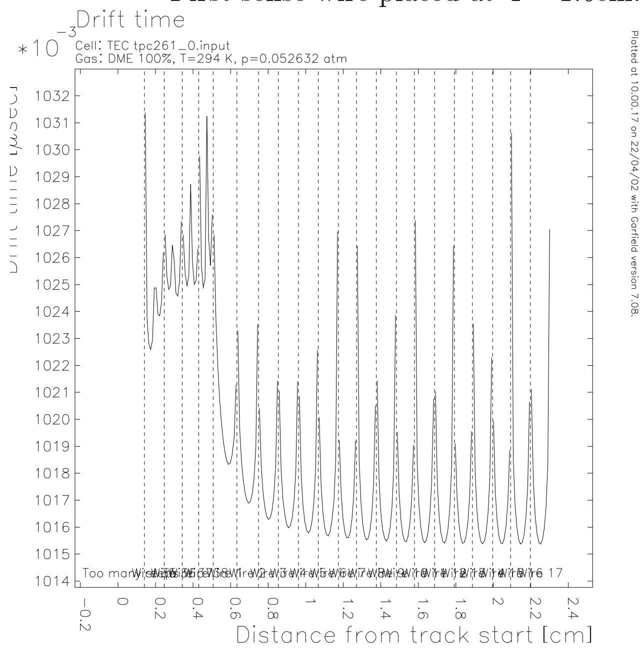

Figure 6: Arrival drift time distribution of electrons from the track presented in Fig.5. First sense wire placed at $X = 0.6cm$ along the horizontal axis. $V_c = -2000V$.

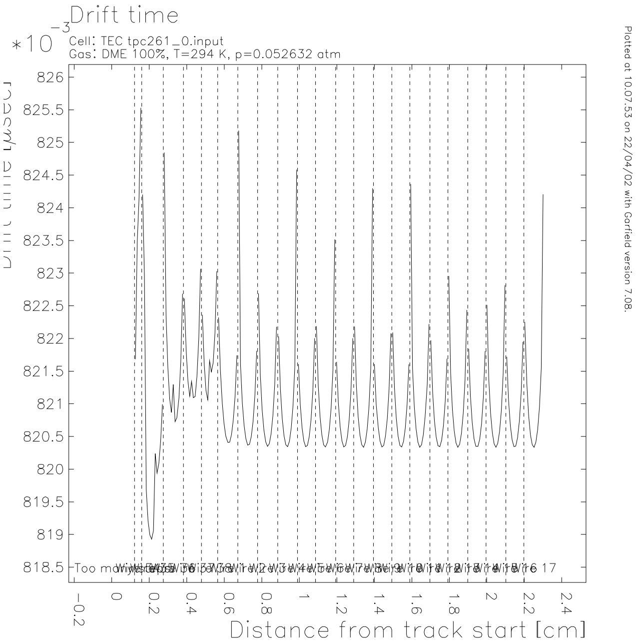

Figure 7: Arrival drift time distribution of electrons from the track presented in Fig.5. First sense wire placed at $X = 0.6cm$ along the horizontal axis. $V_c = -4300V$.

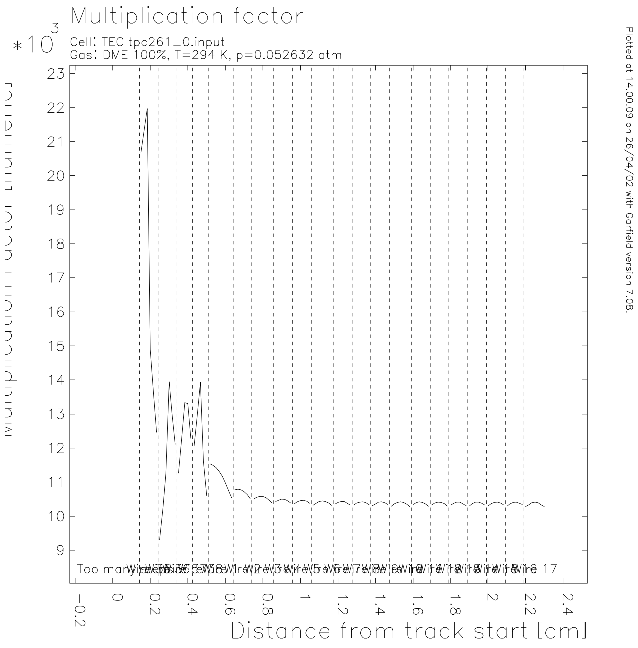

Figure 8: Gain changing near the TEC edge for track presented in Fig.5. DME gas, $V_c = -2000V$, $V_g = 950V$. First sense wire placed at $X = 0.6cm$ along the horizontal axis.

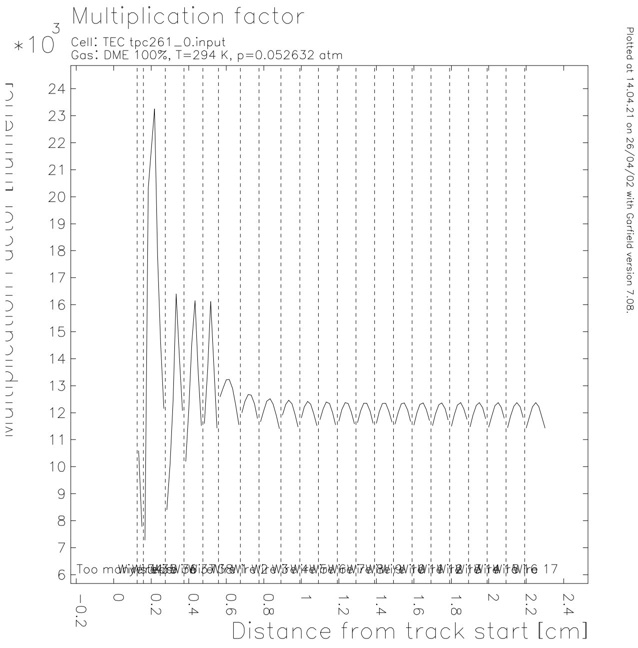

Figure 9: Gain changing near the TEC edge for track presented in Fig.5. DME gas, $V_c = -4300V$, $V_g = 950V$. First sense wire placed at $X = 0.6cm$ along the horizontal axis.

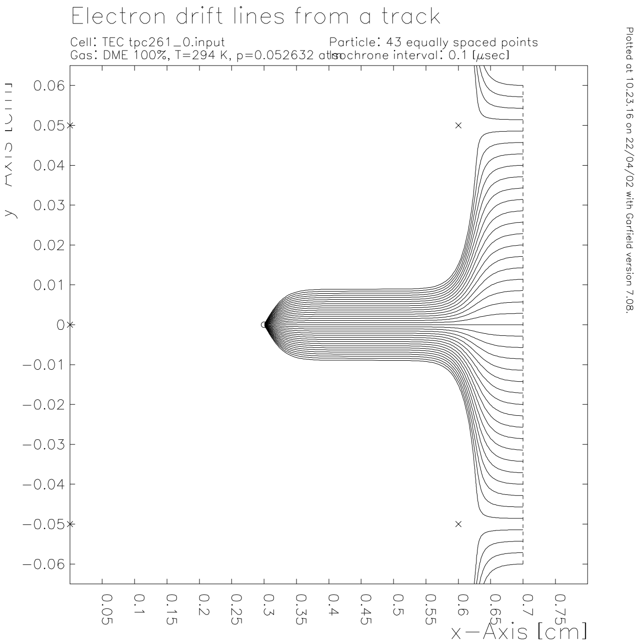

Figure 10: Electron drift lines from a track going at distance of 1mm from the grid wires plane. DME gas, $V_c = -2000V$, $V_g = 950V$.

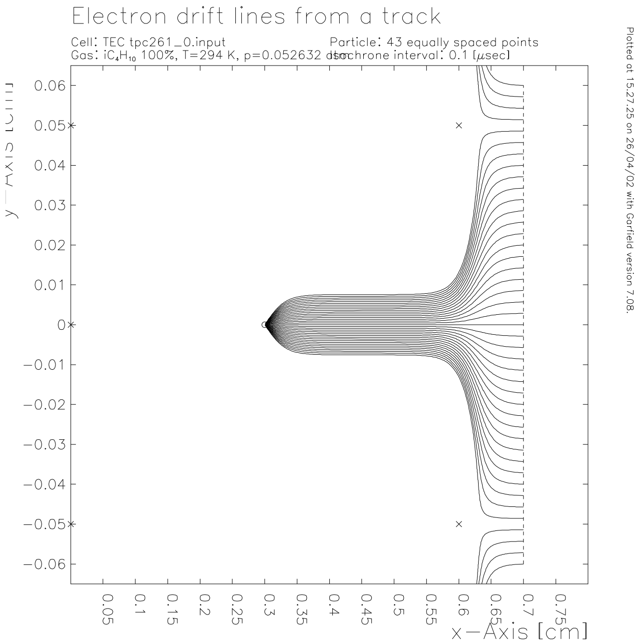

Figure 11: Electron drift lines from a track going at distance of 1mm from the grid wires plane. ISO gas, $V_c = -2000V$, $V_g = 1130V$.

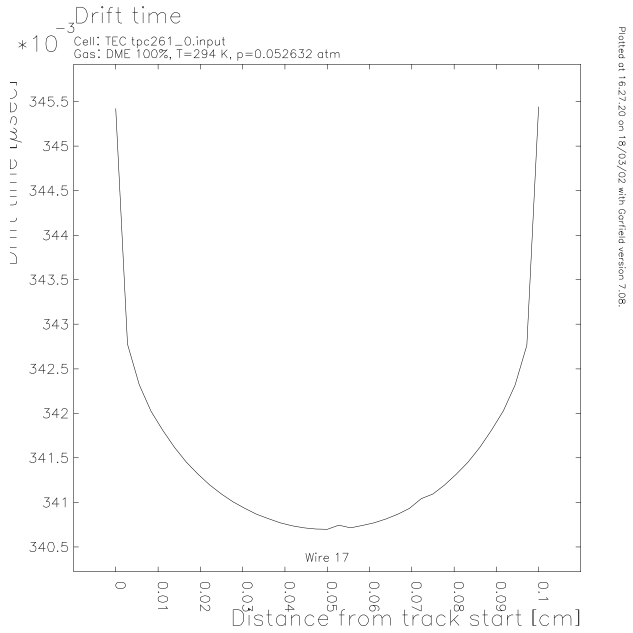

Figure 12: Arrival time distribution of electrons along a track covering central wire cell space. DME gas, $V_c = -2000V$, no diffusion.

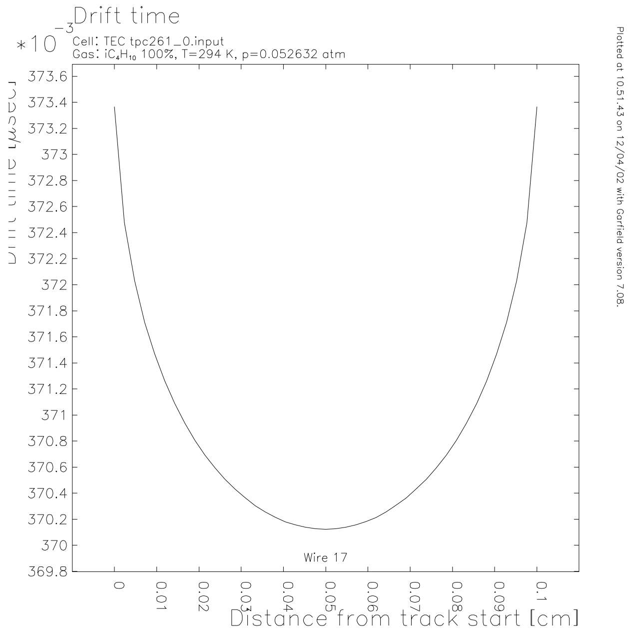

Figure 13: Arrival time distribution of electrons along a track covering central wire cell space. ISO gas, $V_c = -2000V$, no diffusion.

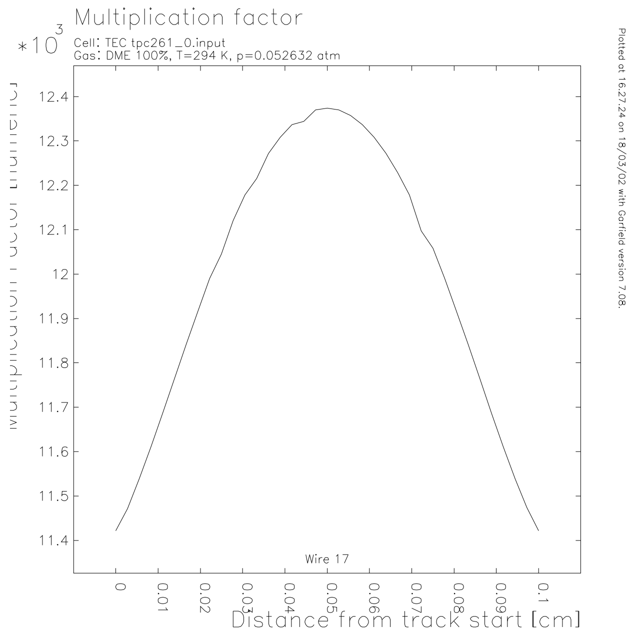

Figure 14: Gain distribution along track covering central wire cell space. DME gas $V_c = -2000V, V_s = 950V$.

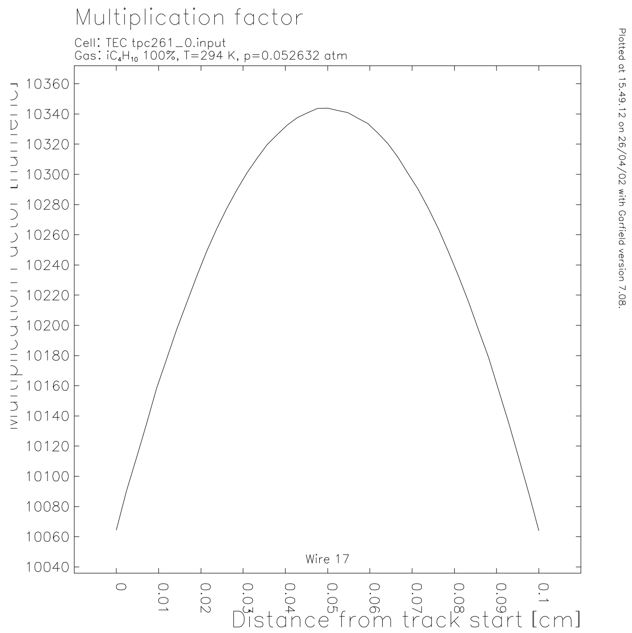

Figure 15: Gain distribution along track covering central wire cell space. ISO gas $V_c = -2000V, V_s = 1130V$.

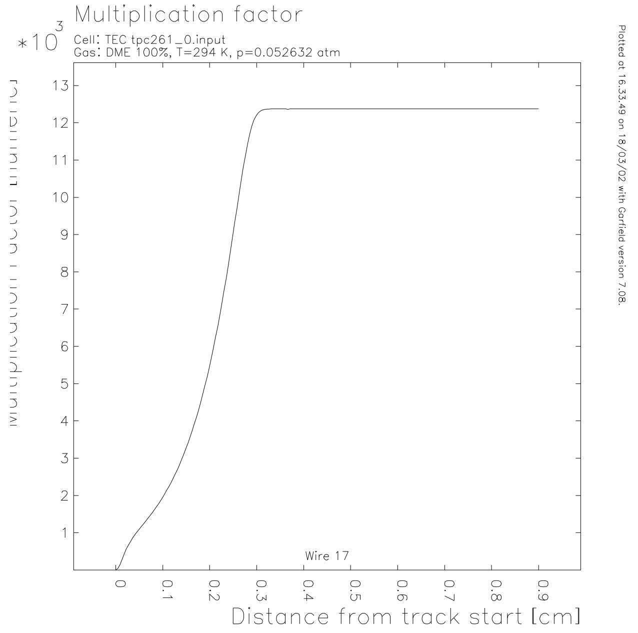

Figure 16: Gain from a track going along $Y = 0$ axis. Grid wire plane placed at $X = 0.3cm$ along horizontal axis. Sense wire placed at $X = 0$. DME gas, $V_c = -2000V, V_g = 950V$.

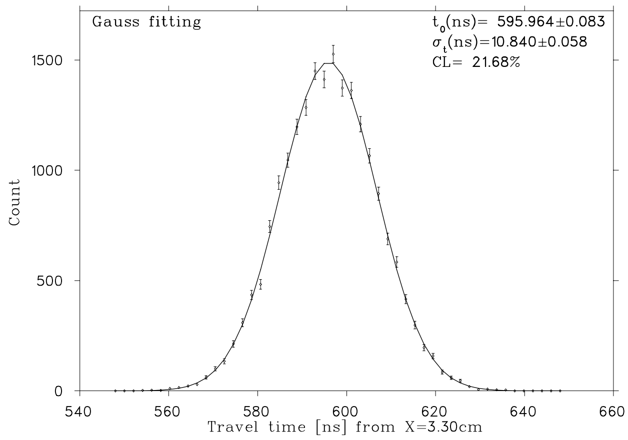

Figure 17: Arrival time distribution of single electrons from a track going at $3.3cm$ from the grid plane along Y-axis. 20000 tracks were simulated.

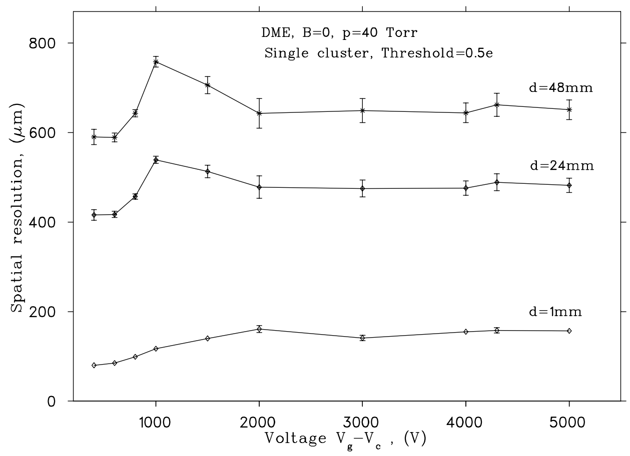

Figure 18: Single electron space resolution of the TEC with DME gas versus $V_g - V_c$ value at several distances d from the grid plane.

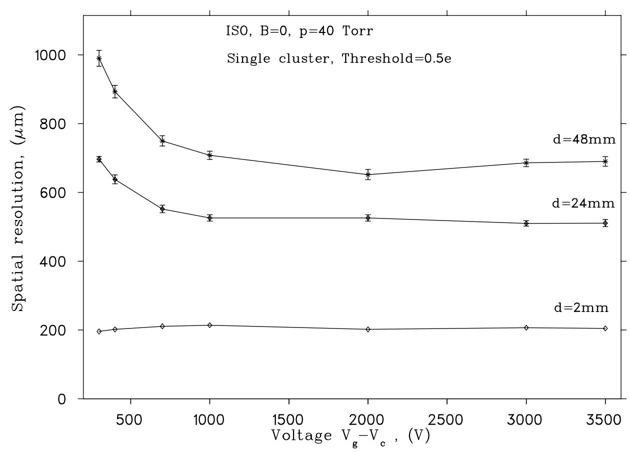

Figure 19: Single electron space resolution of the TEC with ISO gas versus $V_g - V_c$ value at several distances d from the grid plane.

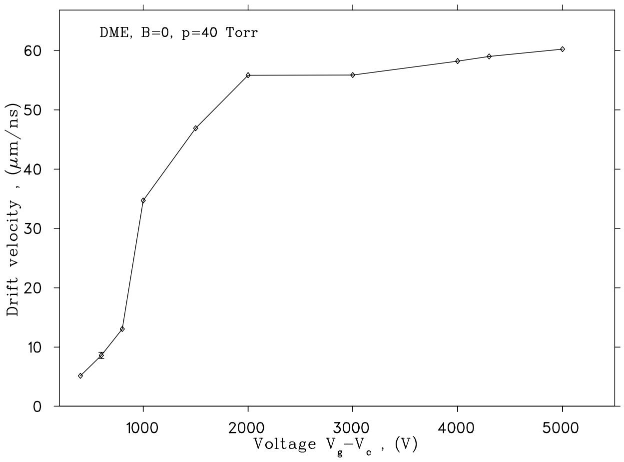

Figure 20: Drift velocity in the TEC with DME gas versus electric field in drift space.

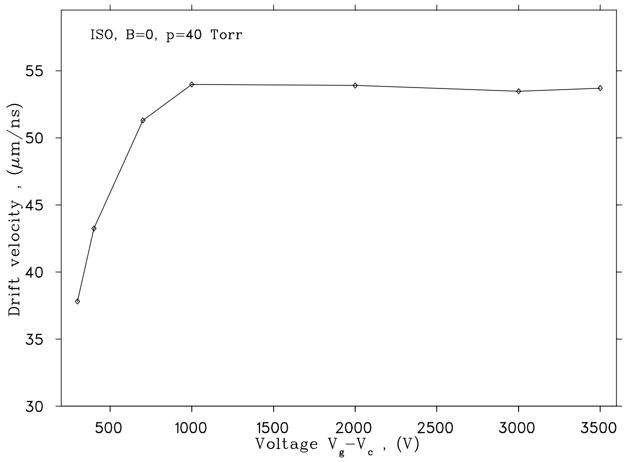

Figure 21: Drift velocity in the TEC with ISO gas versus electric field in drift space.

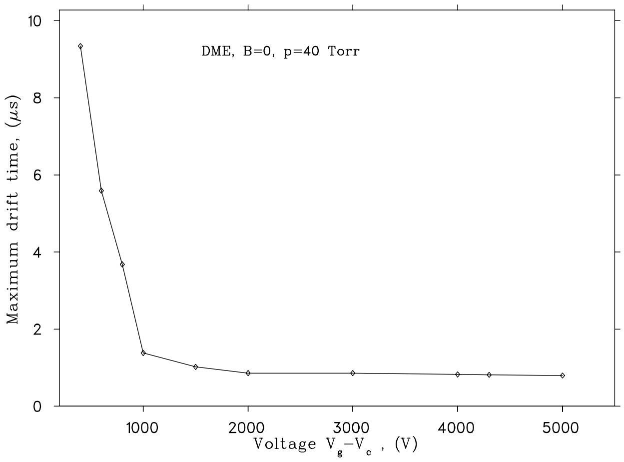

Figure 22: Maximum drift time in the TEC with DME gas vs. value of V_c.

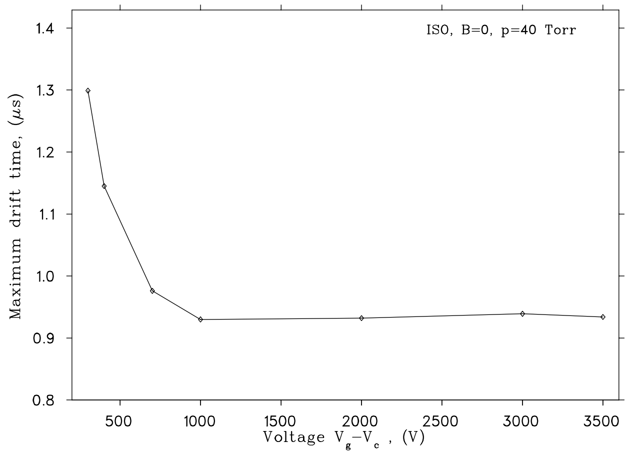

Figure 23: Maximum drift time in the TEC with ISO gas vs. value of V_c.

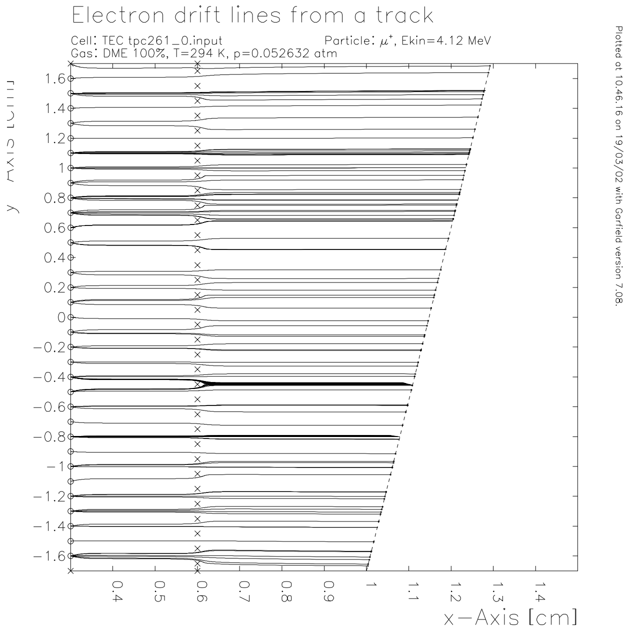

Figure 24: View of a surface muon track and drift electrons in XY-plane. DME gas, $p = 40 Torr$.

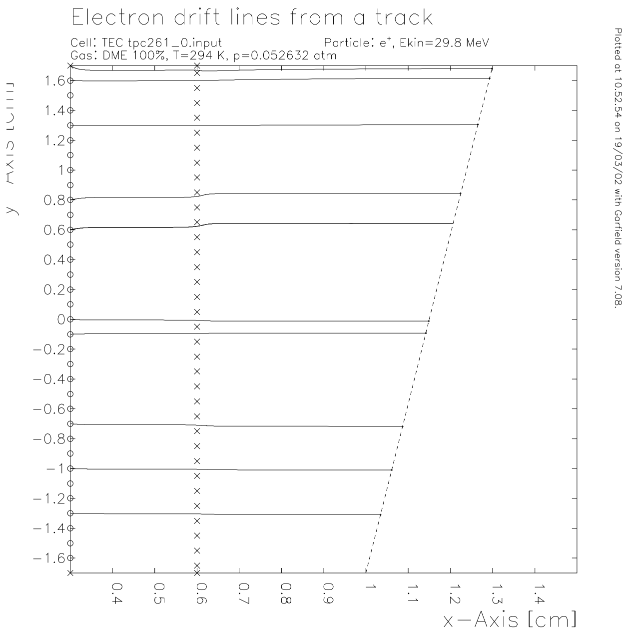

Figure 25: View of positron track and drift electrons in XY-plane at $p = 29.8 MeV/c$. DME gas, $p = 40 Torr$.

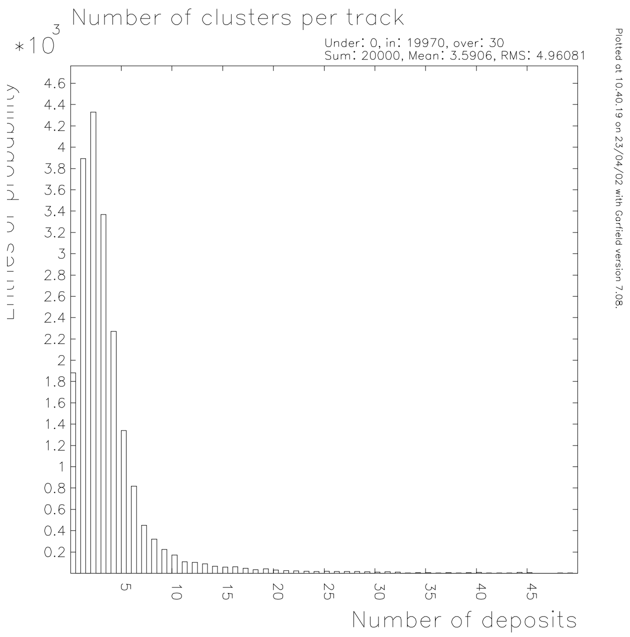

Figure 26: Cluster distribution per $1mm$ from a surface muon in DME gas at $p = 40 Torr$.

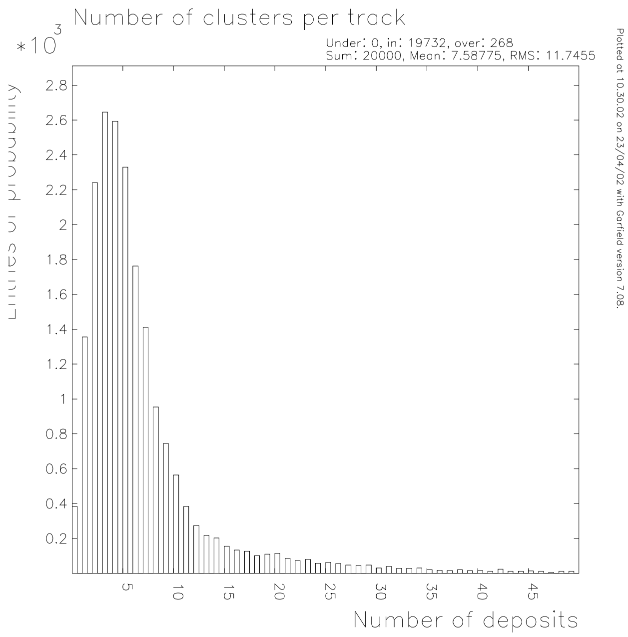

Figure 27: Cluster distribution per $1mm$ from a surface muon in ISO gas at $p = 40 Torr$.

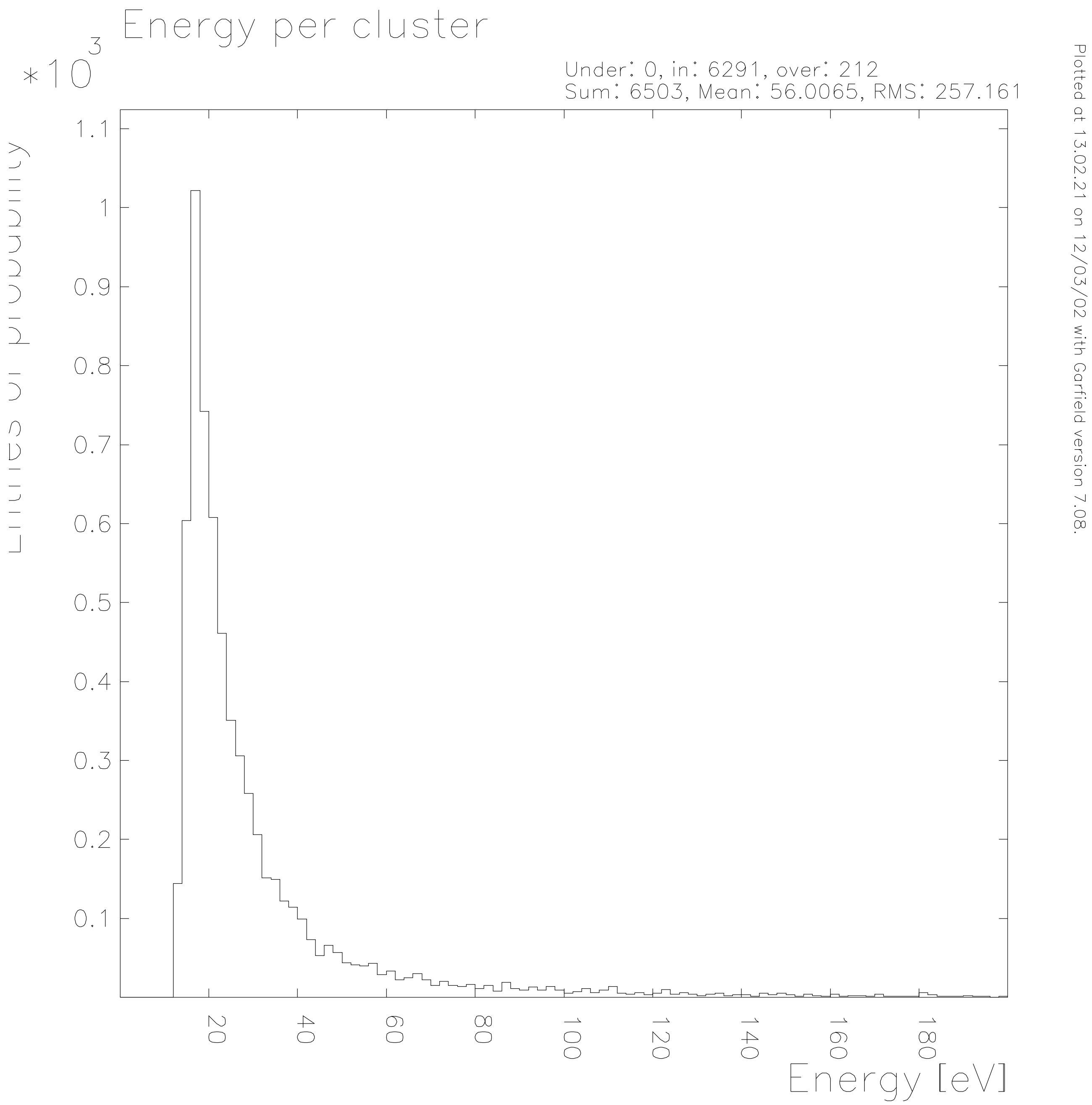

Figure 28: Energy loss distribution of a surface muon per cluster in DME gas at $p = 40 Torr$ calculated by the HEED program.

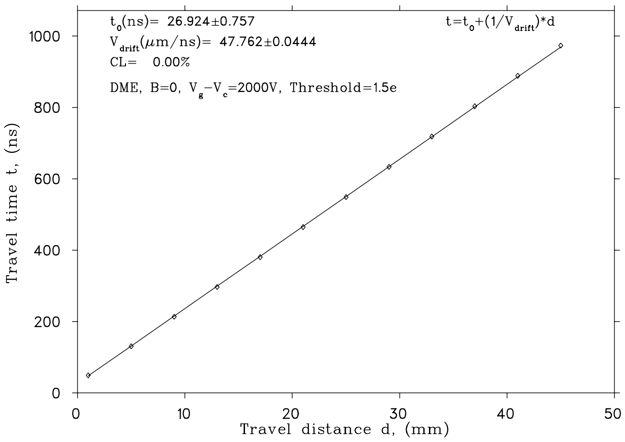

Figure 29: t(x)-relation for TEC with DME gas at $p = 40Torr$.

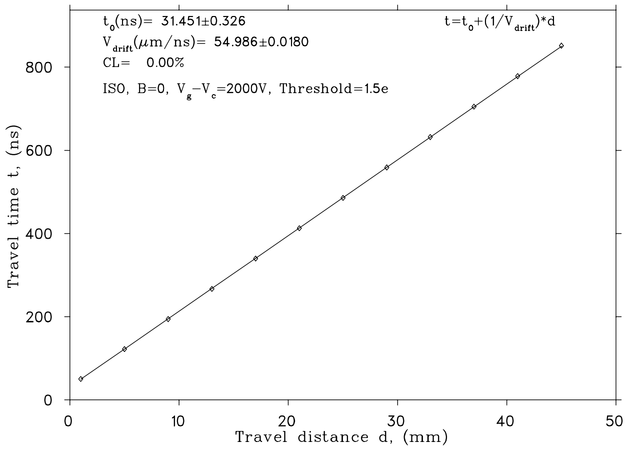

Figure 30: t(x)-relation for for TEC with ISO gas at $p = 40Torr$.

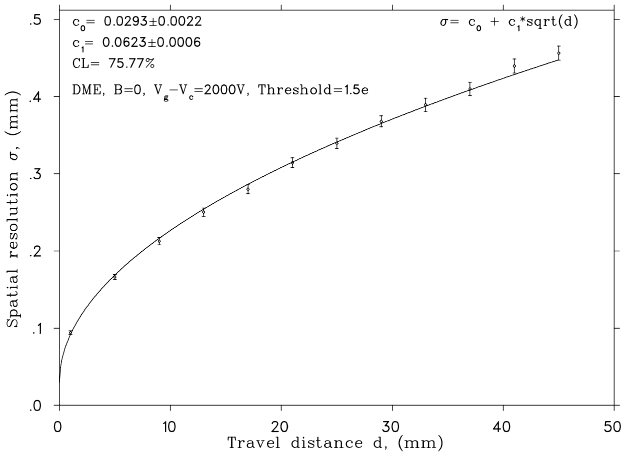

Figure 31: Spatial resolution of the TEC with DME gas at $40Torr$ vs. travel distance d.

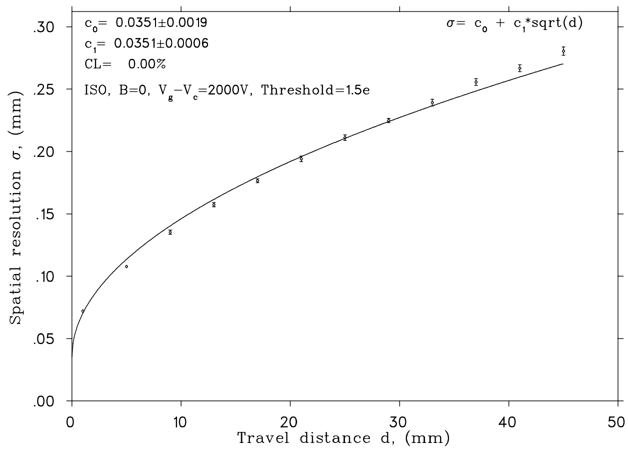

Figure 32: Spatial resolution of the TEC with ISO gas at $p = 40Torr$ vs. travel distance d.

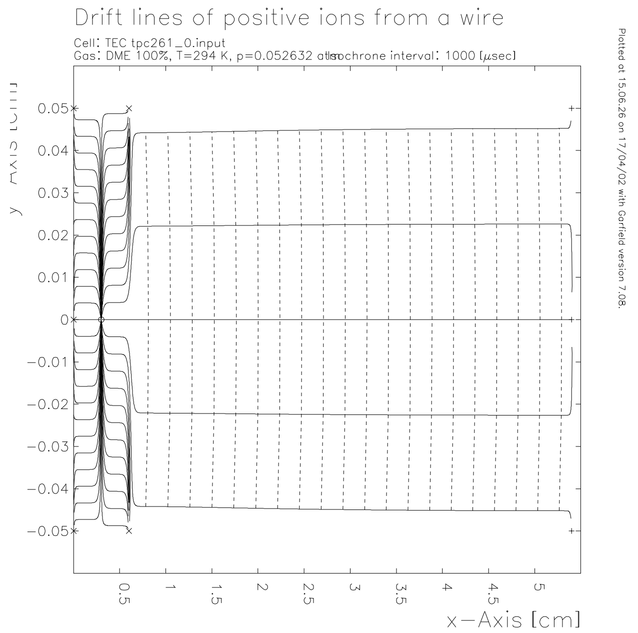

Figure 33: Ion drift lines from a sense wire in TEC with DME gas at $V_c = -2000V$ and B=0.

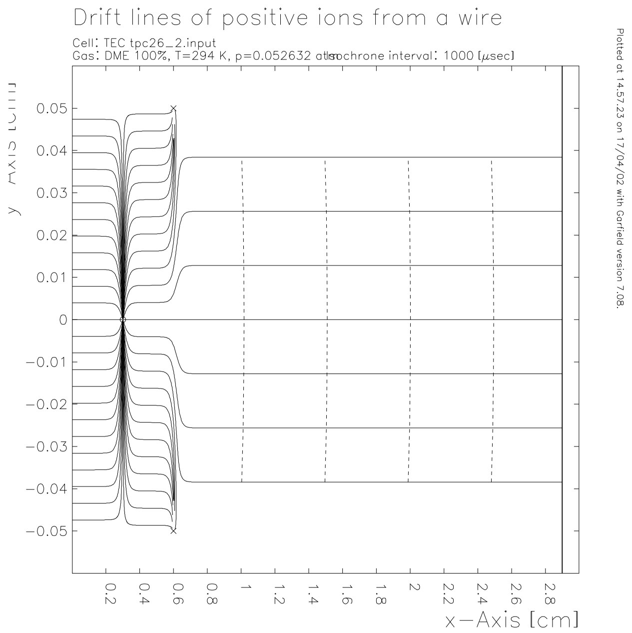

Figure 34: Ion drift lines from a sense wire in TEC with DME gas at $V_c = -2000V$ and B=2T.

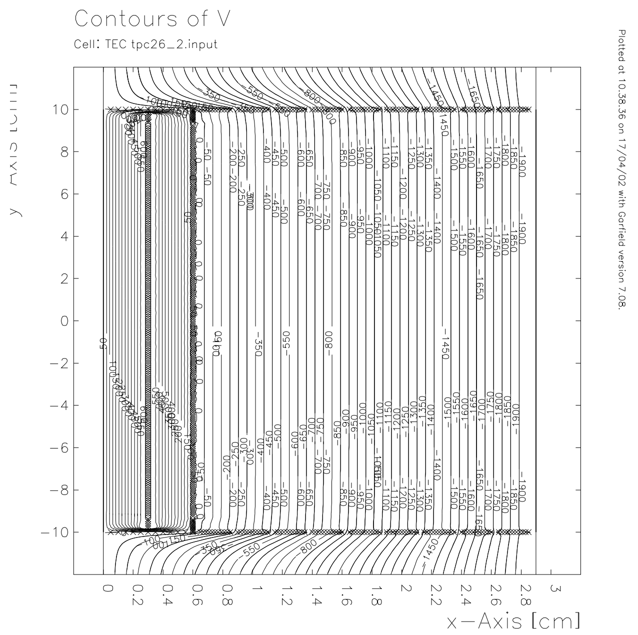

Figure 35: TEC at B=2T together with contours of $V = const$. DME gas, $V_c = -2000V$.

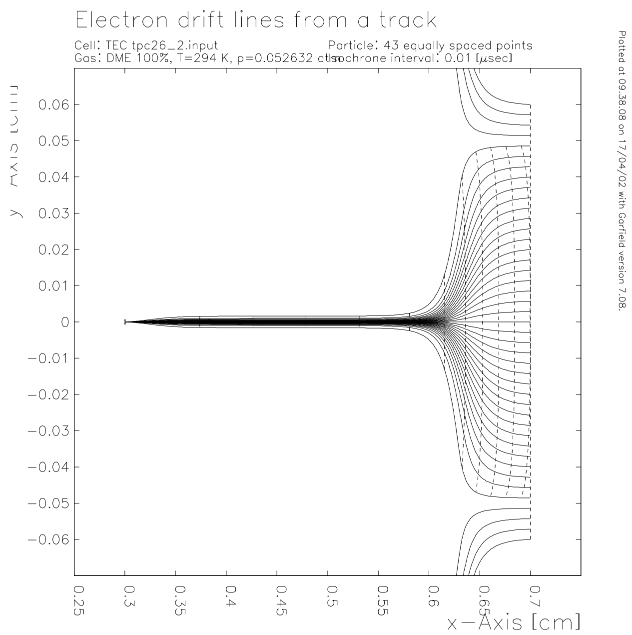

Figure 36: Electron drift lines from a track going at distance of 1mm from the grid wires plane. DME gas, $V_c = -2000V$, $V_g = 950V, B = 2T$.

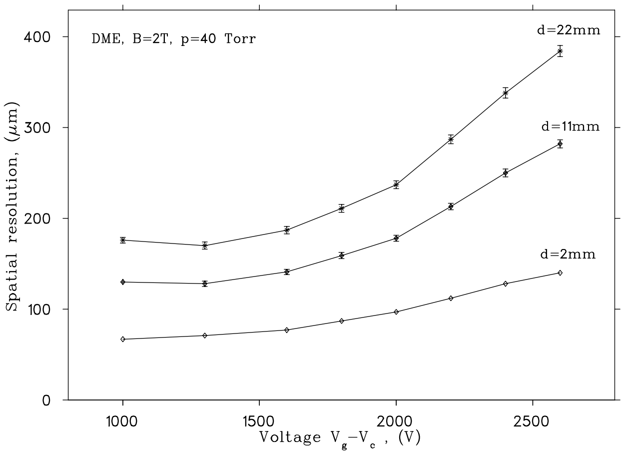

Figure 37: Single electron space resolution of the TEC at B=2T versus value of V_c at several distances d from the grid plane.

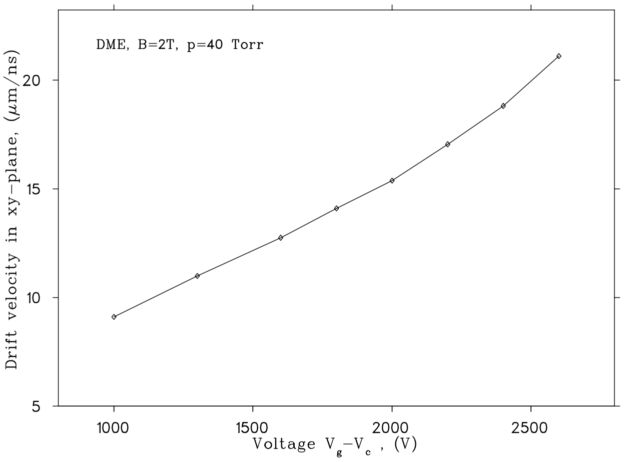

Figure 38: Drift velocity in Z=0 plane in DME gas at B=2T versus value of V_c.

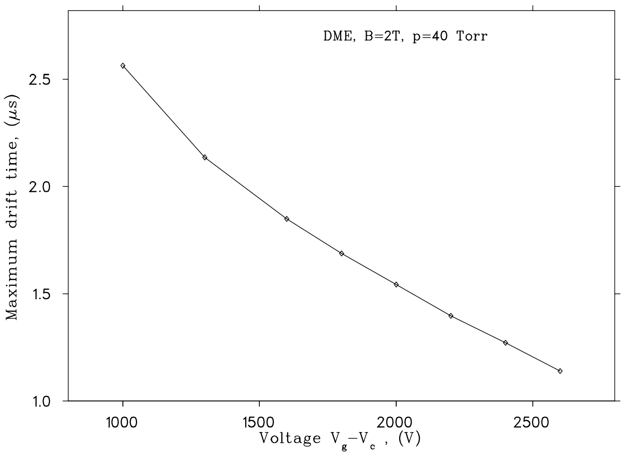

Figure 39: Maximum drift time versus value of V_c. DME gas, $V_c = -2000V$, $V_g = 950V, B = 2T$.

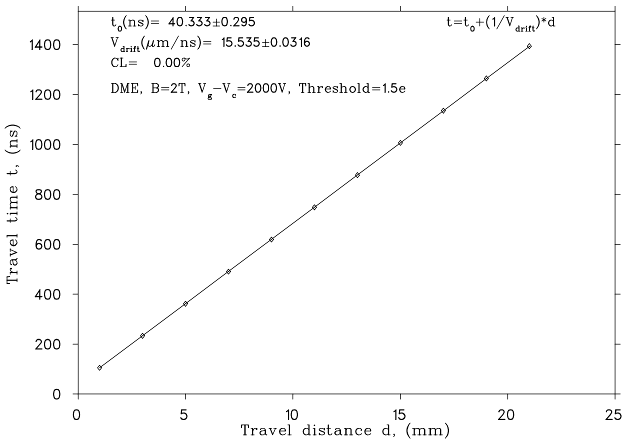

Figure 40: t(x)-relation for TEC with DME gas at B=2T.

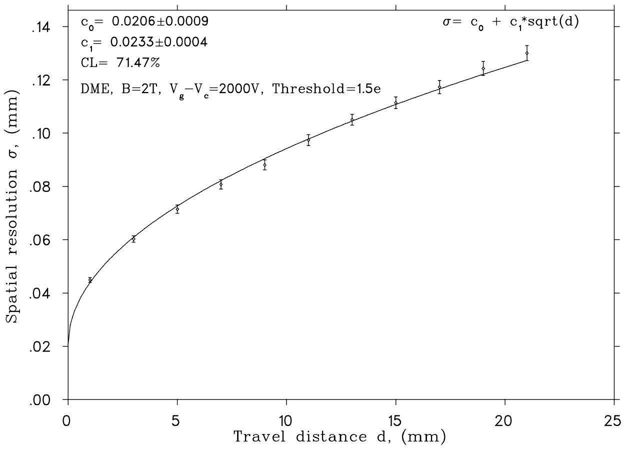

Figure 41: Spatial resolution of the TEC with DME gas at $40Torr$ and B=2T vs. travel distance d.

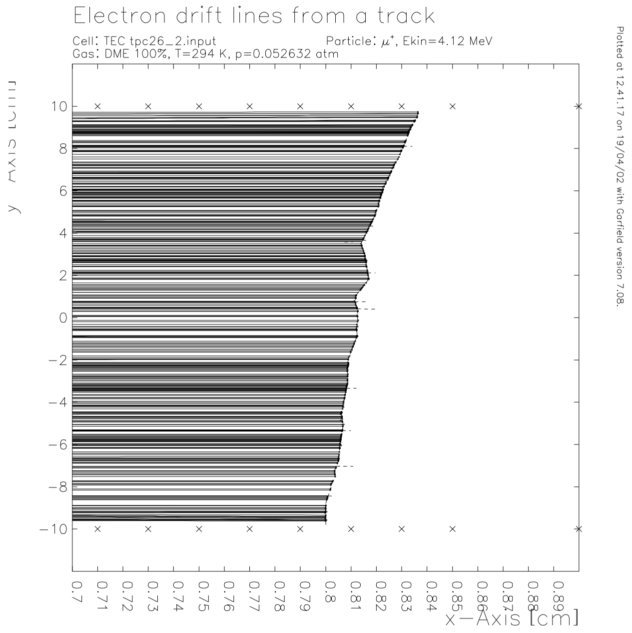

Figure 42: View of a muon track and drift electrons in Z=0 plane. Original track direction is along Y-axis. DME gas, $p = 40Torr$, $B = 2T$.

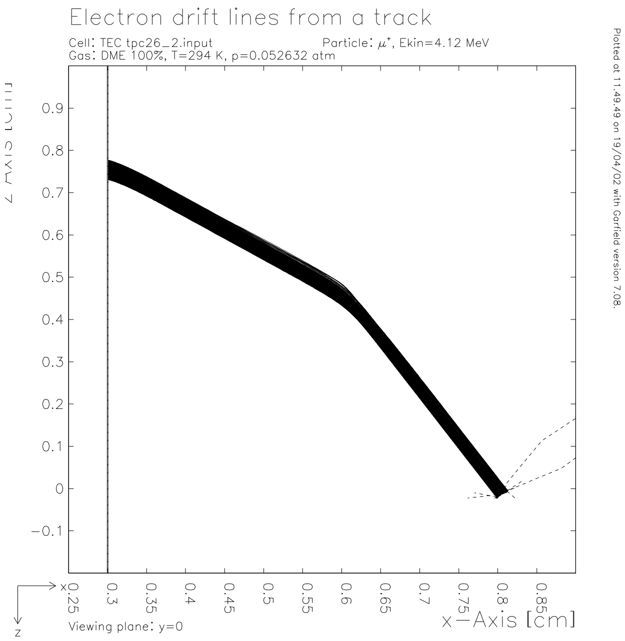

Figure 43: View of a muon track from Fig.42 and drift electrons in Y=0 plane. DME gas, $p = 40Torr$, $B = 2T$. Sense wire placed at $X = 0.3cm$.

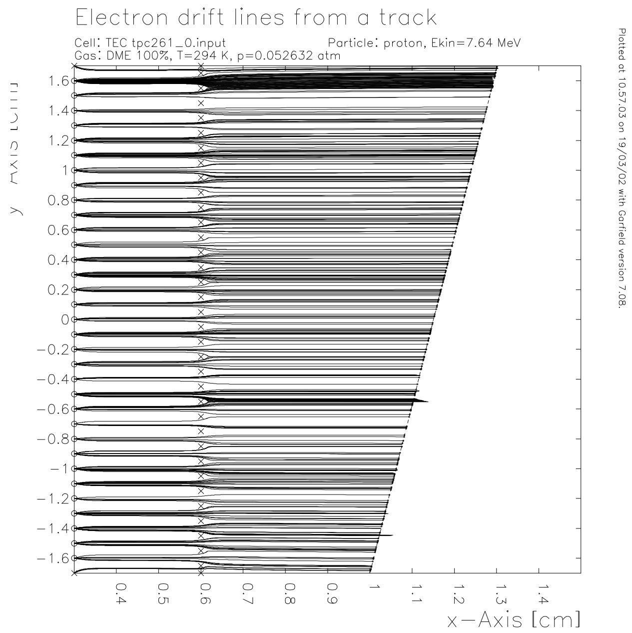

Figure 44: View of a proton track and drift electrons in XY-plane. $p = 120MeV/c$, DME gas, $p = 40Torr, B = 0$.

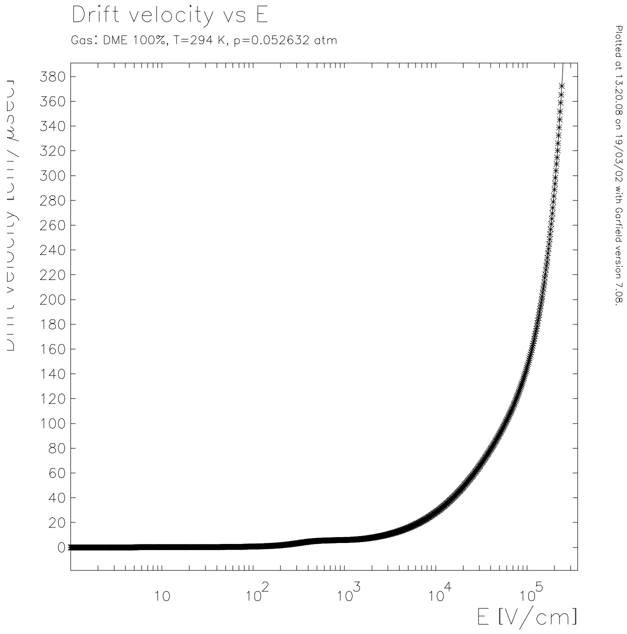

Figure 45: Drift velocity in DME gas at $p = 40Torr$ and B=0 vs. electric field value.

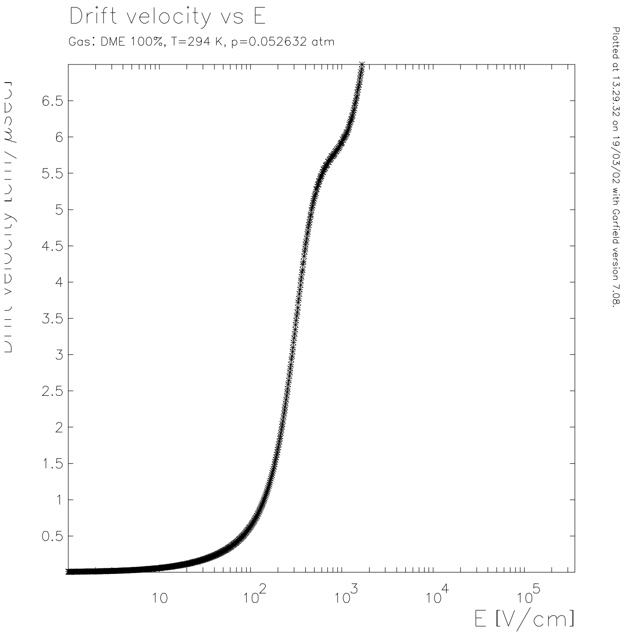

Figure 46: A detailed part of drift velocity dependency in DME gas at B=0 and $p = 40Torr$ from electric field value. Value of $V_c = -2000V$ corresponds to $E = 417V/cm$. Value of $V_c = -4300V$ corresponds to $E = 896V/cm$.

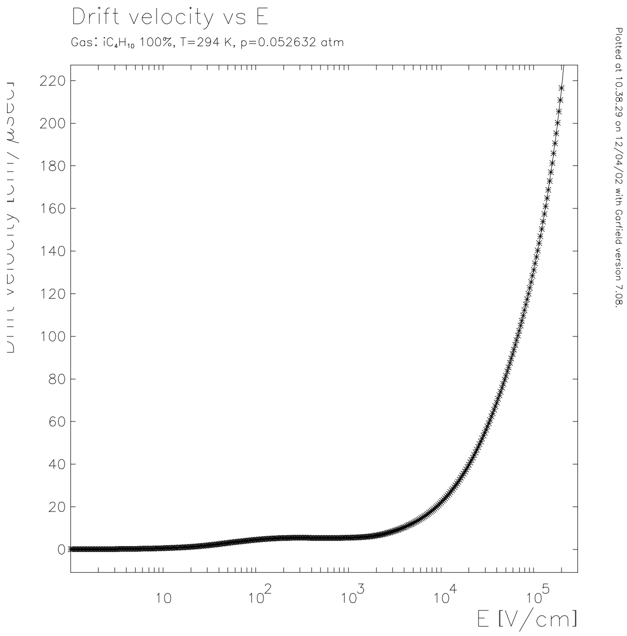

Figure 47: Drift velocity in ISO gas at B=0 and $p = 40Torr$ vs. electric field value.

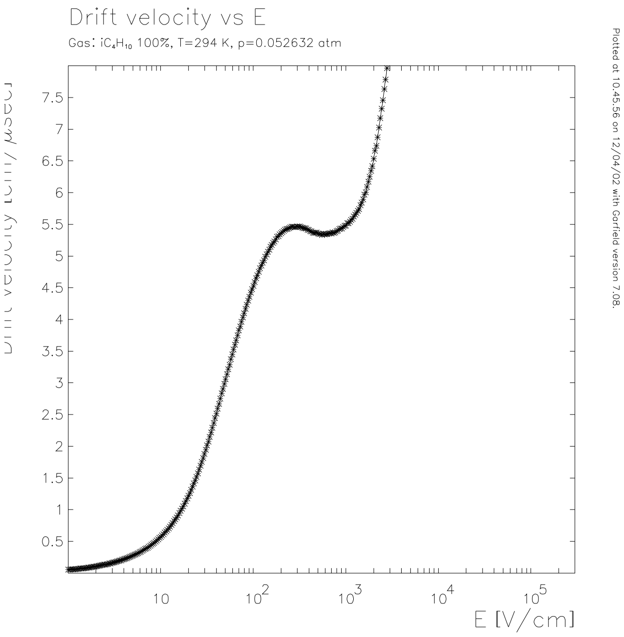

Figure 48: A detailed part of drift velocity dependency in ISO gas at B=0 and $p = 40Torr$ from electric field value. Value of $V_c = -2000V$ corresponds to $E = 417V/cm$.

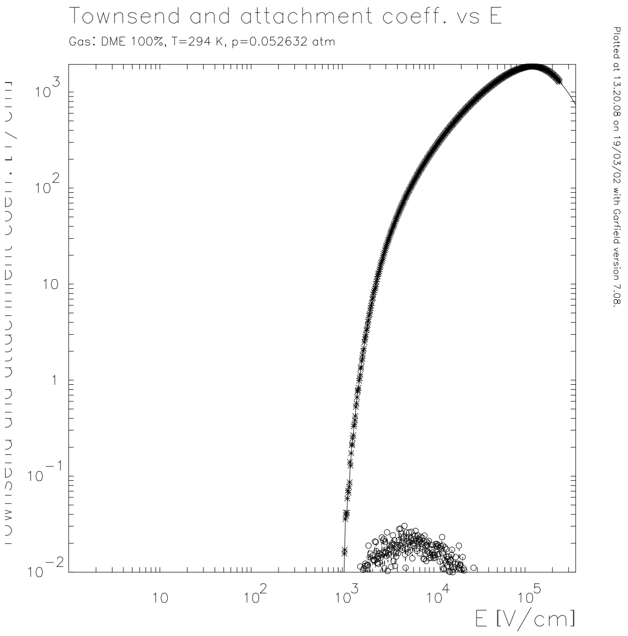

Figure 49: Townsend and attachment coefficients in DME gas at B=0.

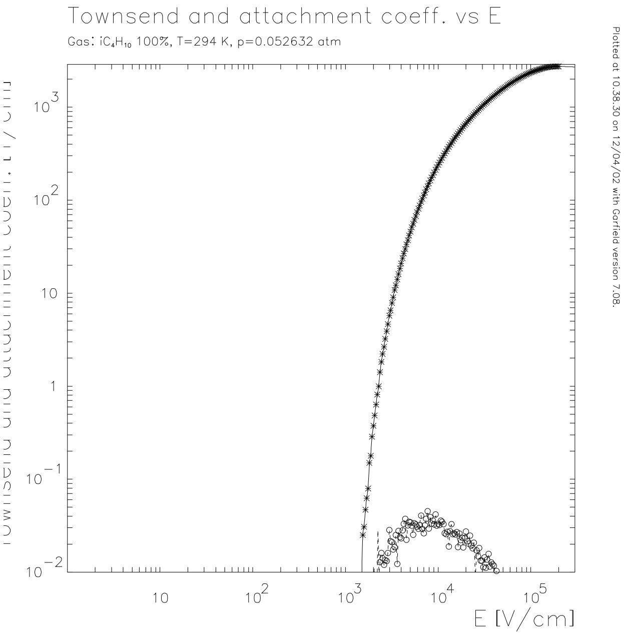

Figure 50: Townsend and attachment coefficients in ISO gas at B=0.

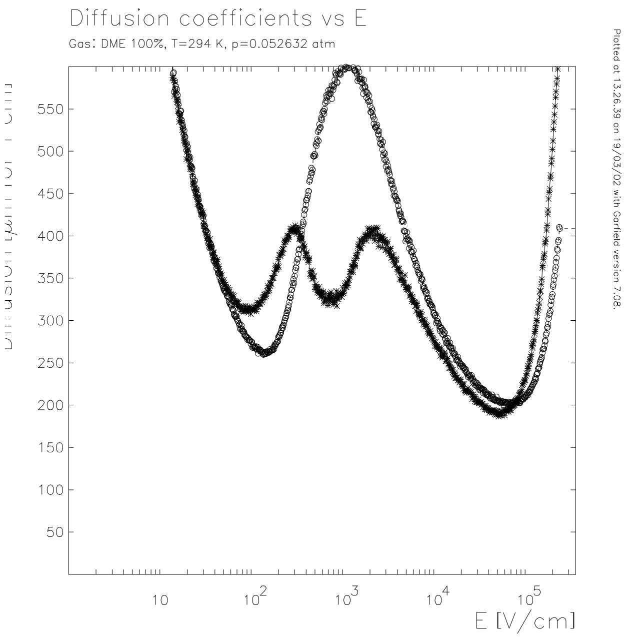

Figure 51: Diffusion coefficients in DME gas at B=0. Value of $V_c = -2000V$ corresponds to $E = 417V/cm$. Value of $V_c = -4300V$ corresponds to $E = 896V/cm$.

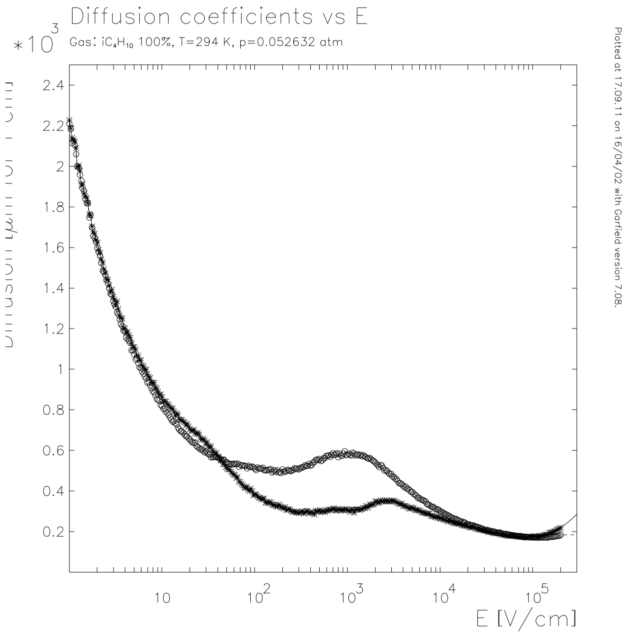

Figure 52: Diffusion coefficients in ISO gas at B=0. Value of $V_c = -2000V$ corresponds to $E = 417V/cm$.

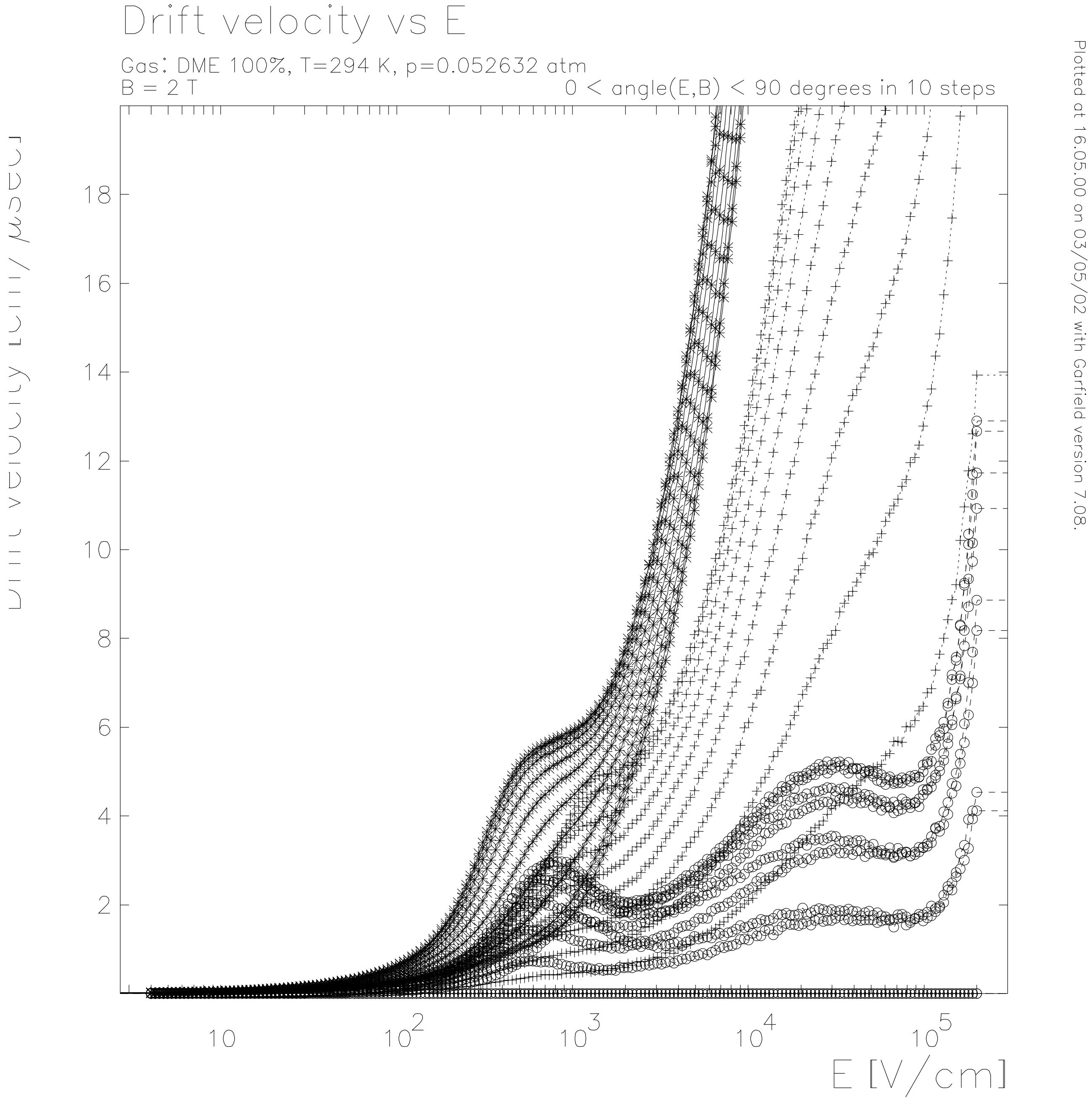

Figure 53: A detailed part of drift velocity dependences in DME gas at B=2T and $p = 40Torr$ from electric field value. Value of $V_c = -2000V$ corresponds to $E = 870V/cm$.

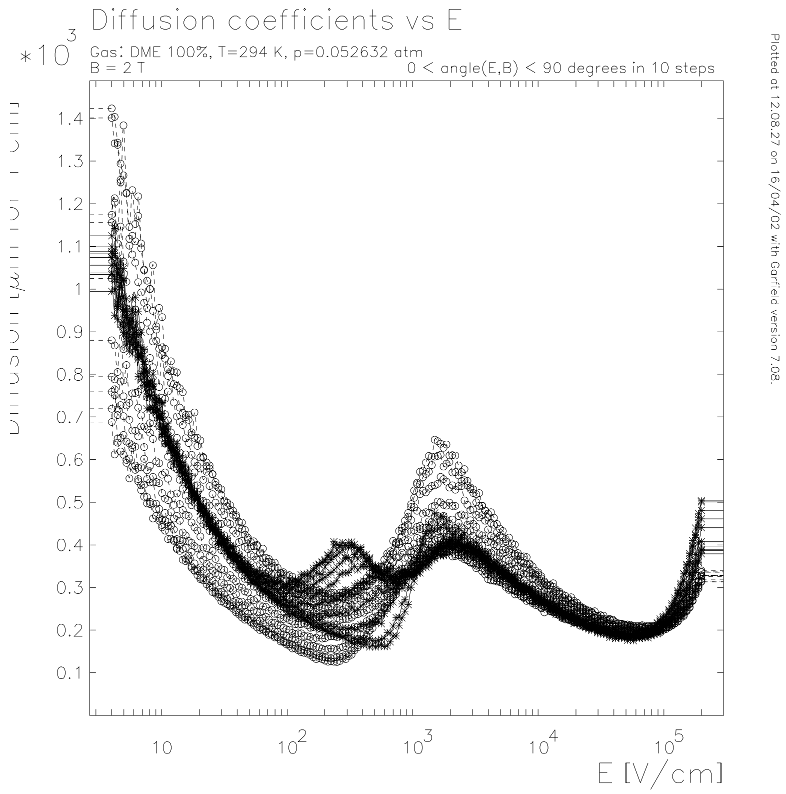

Figure 54: Diffusion coefficients in DME gas at B=2T. Value of $V_c = -2000V$ corresponds to $E = 870V/cm$.

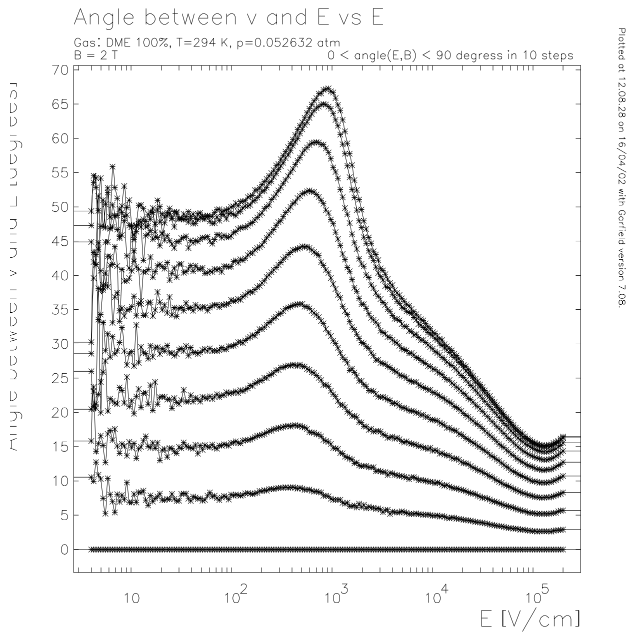

Figure 55: Lorentz drift angle in DME gas at B=2T. Value of $V_c = -2000V$ corresponds to $E = 870V/cm$.

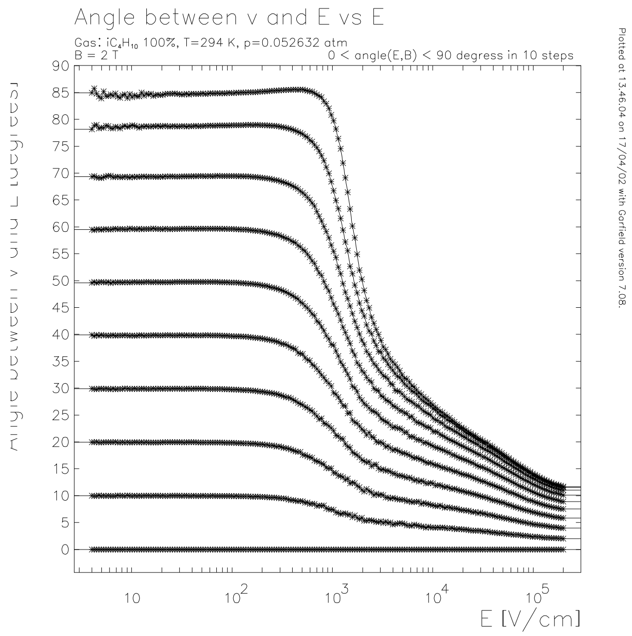

Figure 56: Lorentz drift angle in ISO gas at B=2T. Value of $V_c = -2000V$ corresponds to $E = 870V/cm$.